12-03 December 2003

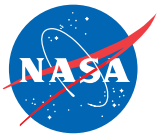

TECH BRIEFS

NATIONAL AERONAUTICS AND SPACE ADMINISTRATION

INTRODUCTION

Tech Briefs are short announcements of innovations originating from research and development activities of the National Aeronautics and Space Administration. They emphasize information considered likely to be transferable across industrial, regional, or disciplinary lines and are issued to encourage commercial application.

Availability of NASA Tech Briefs and TSPs

Requests for individual Tech Briefs or for Technical Support Packages (TSPs) announced herein should be addressed to

National Technology Transfer Center

Telephone No. **(800) 678-6882** or via World Wide Web at **www2.nttc.edu/leads/**

Please reference the control numbers appearing at the end of each Tech Brief. Information on NASA's Commercial Technology Team, its documents, and services is also available at the same facility or on the World Wide Web at **www.nctn.hq.nasa.gov**.

Commercial Technology Offices and Patent Counsels are located at NASA field centers to provide technology-transfer access to industrial users. Inquiries can be made by contacting NASA field centers and program offices listed below.

NASA Field Centers and Program Offices

Ames Research Center
Carolina Blake
(650) 604-1754
carolina.m.blake@nasa.gov

Dryden Flight Research Center
Jenny Baer-Riedhart
(661) 276-3689
jenny.baer-riedhart@dfrc.nasa.gov

Goddard Space Flight Center
Nona Cheeks
(301) 286-5810
Nona.K.Cheeks.1@gsfc.nasa.gov

Jet Propulsion Laboratory
Art Murphy, Jr.
(818) 354-3480
arthur.j.murphy-jr@jpl.nasa.gov

Johnson Space Center
Charlene E. Gilbert
(281) 483-3809
commercialization@jsc.nasa.gov

Kennedy Space Center
Jim Aliberti
(321) 867-6224
Jim.Aliberti-1@ksc.nasa.gov

Langley Research Center
Jesse Midgett
(757) 864-3936
jesse.c.midgett@nasa.gov

John H. Glenn Research Center at Lewis Field
Larry Viterna
(216) 433-3484
cto@grc.nasa.gov

Marshall Space Flight Center
Vernotto McMillan
(256) 544-2615
vernotto.mcmillan@msfc.nasa.gov

Stennis Space Center
Robert Bruce
(228) 688-1929
robert.c.bruce@nasa.gov

NASA Program Offices

At NASA Headquarters there are seven major program offices that develop and oversee technology projects of potential interest to industry:

Carl Ray
Small Business Innovation Research Program (SBIR) & Small Business Technology Transfer Program (STTR)
(202) 358-4652 or
cray@mail.hq.nasa.gov

Benjamin Neumann
InnovativeTechnology Transfer Partnerships (Code RP)
(202) 358-2320
benjamin.j.neumann@nasa.gov

John Mankins
Office of Space Flight (Code MP)
(202) 358-4659 or
jmankins@mail.hq.nasa.gov

Terry Hertz
Office of Aero-Space Technology (Code RS)
(202) 358-4636 or
thertz@mail.hq.nasa.gov

Glen Mucklow
Office of Space Sciences (Code SM)
(202) 358-2235 or
gmucklow@mail.hq.nasa.gov

Roger Crouch
Office of Microgravity Science Applications (Code U)
(202) 358-0689 or
rcrouch@hq.nasa.gov

Granville Paules
Office of Mission to Planet Earth (Code Y)
(202) 358-0706 or
gpaules@mtpe.hq.nasa.gov

TECH BRIEFS

NATIONAL AERONAUTICS AND SPACE ADMINISTRATION

Organic/Inorganic Hybrid Polymer/Clay Nanocomposites

The exfoliation and dispersion of clay particles are improved.

Langley Research Center, Hampton, Virginia

A novel class of polymer/clay nanocomposites has been invented in an attempt to develop transparent, lightweight, durable materials for a variety of aerospace applications. As their name suggests, polymer/clay nanocomposites comprise organic/inorganic hybrid polymer matrices containing platelet-shaped clay particles that have sizes of the order of a few nanometers thick and several hundred nanometers long. Partly because of their high aspect ratios and high surface areas, the clay particles, if properly dispersed in the polymer matrix at a loading level of 1 to 5 weight percent, impart unique combinations of physical and chemical properties that make these nanocomposites attractive for making films and coatings for a variety of industrial applications. Relative to the unmodified polymer, the polymer/clay nanocomposites may exhibit improvements in strength, modulus, and toughness; tear, radiation, and fire resistance; and lower thermal expansion and permeability to gases while retaining a high degree of optical transparency.

The clay particles of interest occur naturally as layered silicates. In order to fully realize the benefits of a polymer/clay nanocomposite, it is necessary that the clay particles become fully exfoliated (delaminated) and uniformly dispersed in the polymer matrix. Concomitantly, it is necessary to maintain the exfoliation, counteracting a tendency, observed in prior formulations of polymer/clay nanocomposites, for dispersions of exfoliated clay particles to collapse back into stacked layers upon thermal treatment. One reason for the difficulty in achieving and maintaining exfoliation and uniform dispersion is the incompatibility between the silicate particle surfaces (which are hydrophilic) and the polymer matrix (which is hydrophobic). The present invention addresses these issues.

The figure depicts a process for making a polymer/clay nanocomposite film according to the invention. In one of two branches of the first step, a hybrid organic/inorganic matrix resin in a sol-gel form is prepared. The organic precursor of the hybrid is a compound or oligomer that contains both a cross-linkable functional group (e.g., phenylethynyl) and an alkoxysilane group. The inorganic precursor of the hybrid is also an alkoxysilane. Both precursors are mixed with a solvent to form the sol-gel matrix resin. In the other branch of the first step, a clay solution is prepared by initially dispersing layered clay particles in the same solvent as that used to form the sol-gel matrix resin. To achieve intercalation of the solvent into the stacked layers, the mixture is subjected to high-shear mixing and to ultrasound. Suitable clays to provide compatibility to the organic polymer include chemically modified organophilic cation-exchanged smectite type clays and synthetic clays having hydroxyl functional groups on the edges and/or elsewhere on the surfaces of the particles.

In the second step of the process, the clay solution is added to the hybrid sol-gel solution and the resulting mixture subjected to high-shear mixing and ultrasound. The hydroxyl groups of the organic/inorganic hybrid react with hydroxyl groups on the surfaces and the edges of the exfoliated clay particles, forming covalent and/or hydrogen bonds that enhance exfoliation in the presence of high shear.

The third step involves a film casting process. For example, to make an unoriented film, one begins by simply casting the solution onto a glass plate or other suitable clean, dry surface. The solution is allowed to dry to a tack-free film in ambient, desiccated air, then further dried and cured in flowing heated air. During this thermal treatment, the remaining silanol groups of the hybrid undergo condensation reactions, forming a molecular network that prevents the reunion of the exfoliated particles into stacked layers. In addition, the organic matrix can be consolidated with further crosslinking among the cross-linkable functional groups during thermal cure. It may be possible to prepare oriented films and fibers by using shear, drawing, and fiber spinning processes.

This work was done by Cheol Park (NRC), John W. Connell, and Joseph G. Smith, Jr., of **Langley Research Center**. *For further information, contact the Langley Commercial Technology Office at (757) 864-3936.*
LAR-16216

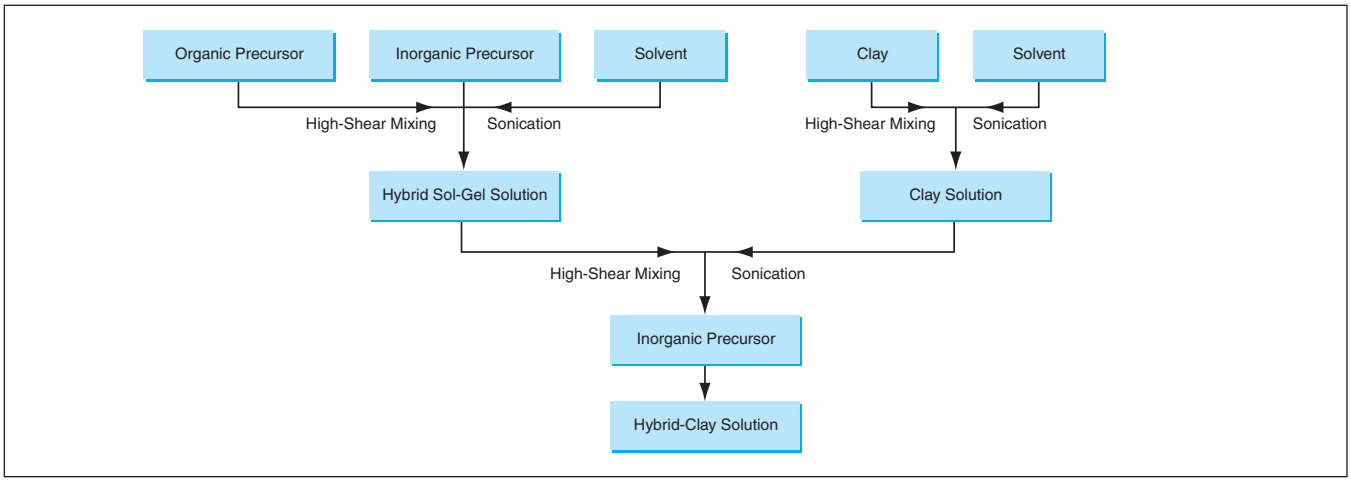

This **Flow Diagram** shows the major steps of a process for making a film of an organic/inorganic hybrid polymer/clay nanocomposite.

Less-Toxic Coatings for Inhibiting Corrosion of Aluminum

It is no longer necessary to use highly toxic and carcinogenic chromates.

John F. Kennedy Space Center, Florida

Two recently invented families of conversion-coating processes have been found to be effective in reducing or preventing corrosion of aluminum alloys. These processes offer less-toxic alternatives to prior conversion-coating processes that are highly effective but have fallen out of favor because they generate chromate wastes, which are toxic and carcinogenic. Specimens subjected to these processes were found to perform well in standard salt-fog corrosion tests.

One family of processes is based on the treatment of suitably prepared aluminum-alloy workpieces with calcium hydroxide (lime) solutions. Preparation of a workpiece usually includes the following steps: (1) degreasing (e.g., by use of a solvent), (2) cleaning by use of a commercially available alkaline solution, (3) rinsing in water, (4) treatment with a commercially available deoxidizing solution, and (5) optionally coating with boehmite [$AlO_x(OH)_y$] and with transition-metal oxyanions that can include molybdates and/or permanganates, among others. The prepared workpiece is then treated in an aqueous conversion solution that contains between 0.06 and 0.15 weight percent of $Ca(OH)_2$ plus between 0.4 and 5 weight percent of alkali-metal nitrates. Typically, this treatment lasts between 2 and 20 minutes, during which the temperature of the solution is maintained between 50 and 100 °C.

The success of the process depends on the use of a freshly prepared conversion solution: The solution should be made by use of deionized water and should be heated to the treatment temperature before adding the $Ca(OH)_2$. Immediately before immersing the workpiece in the solution, the required amount of $Ca(OH)_2$ should be added.

Optionally, the workpiece can be post-treated to seal the conversion coat and contribute some additional resistance to corrosion. Suitable post-treatment sealing solutions include silicates, borates, and phosphates of alkali metals. The concentrations of the solutes in the sealing solutions can range from 0.05 to 10 weight percent, treatment times can range from 2 to 10 minutes, and treatment temperatures can range from 50 to 80 °C. Finally, the workpiece is rinsed with deionized water, then dried in air for several days.

The other family of processes is based on the treatment of suitably prepared aluminum-alloy workpieces with conversion solutions that contain molybdate (MoO_4^{2-}) ions. The preparation of a workpiece for a process in this family is similar to that for a $Ca(OH)_2$ conversion-coating process: The workpiece is degreased and otherwise cleaned, deoxidized, and coated with boehmite. The prepared workpiece is then treated in an aqueous conversion solution that contains between 1 and 3 weight percent of molybdate ions plus, optionally, small percentages of any or all of the following ingredients: fluorides, oxyanions associated with high-valence transition-metal cations, silicates, borates, phosphates, and/or nitrates. Typically, the treatment lasts between 1 and 60 minutes, during which the temperature of the conversion solution is maintained between 25 and 100 °C and the pH of the solution is maintained between about 10 and 12, the exact value depending on the composition of the solution.

As in the family of $Ca(OH)_2$ conversion-coating processes described above, the workpiece can be post-treated to seal the conversion coat and increase resistance to corrosion. One suitable post-treatment process involves the use of a $Ca(OH)_2$ conversion-coating solution as described above. Other suitable post-treatment solutions include silicates, borates, and phosphates of alkali metals — solutions like those mentioned above for post-treatment following $Ca(OH)_2$ conversion coating. The concentrations of the solutes in these sealing solutions can range from 4 to 10 weight percent, treatment times can range from 5 to 20 minutes, and treatment temperatures can range from 25 to 98 °C. Then, as described above, the post-treated workpiece is rinsed in deionized water and dried in air.

This work was done by Zoran Minevski, Eric Clarke, Cahit Eylem, Jason Maxey, and Carl Nelson of Lynntech, Inc., for **Kennedy Space Center**.

In accordance with Public Law 96-517, the contractor has elected to retain title to this invention. Inquiries concerning rights for its commercial use should be addressed to:

Zoran Minevski
Lynntech, Inc.
7610 Eastmark Drive
Suite 202
College Station, TX 77840
Tel. No.: (979) 693-0017
E-mail: zoran.minevski@lynntech.com

Refer to KSC-12114/15, volume and number of this NASA Tech Briefs *issue, and the page number.*

Liquid Coatings for Reducing Corrosion of Steel in Concrete

Structures could be protected more easily and less expensively.

John F. Kennedy Space Center, Florida

Inorganic coating materials are being developed to slow or stop corrosion of reinforcing steel members inside concrete structures. It is much simpler and easier to use these coating materials than it is to use conventional corrosion-inhibiting systems based on impressed electric currents. Unlike impressed electrical corrosion-inhibiting systems, these coatings do not require continuous consumption of electrical power and maintenance of power-supply equipment. Whereas some conventional systems involve the use of expensive arc-spray equipment to apply the metallic zinc used as the sacrificial anode material, the developmental coatings can be applied by use of ordinary paint sprayers.

A coating material of the type under development is formulated as a liquid containing blended metallic particles and/or moisture-attracting compounds. The liquid mixture is sprayed onto a con-

crete structure. Experiments have shown that even though such a coat resides on the exterior surface, it generates a protective galvanic current that flows to the interior reinforcing steel members. By effectively transferring the corrosion process from the steel reinforcement to the exterior coating, the protective current slows or stops corrosion of the embedded steel. Specific formulations have been found to meet depolarization criteria of the National Association of Corrosion Engineers (NACE) for complete protection of steel reinforcing bars ("rebar") embedded in concrete.

A coating of this type can be applied thick enough to afford protection for ten years or longer. The coating can easily be maintained or replaced to ensure continued protection of the reinforcing steel for an indefinite time.

The costs of protecting structures by use of these coating materials are expected to be less than (or in some cases, comparable to) the costs of protection by most conventional methods:

- Typical costs of installing impressed-electric-current systems range from 10 to 30 dollars per square foot (about 110 to 330 dollars per square meter) [prices as of year 2000]. After installation, these systems incur additional costs of electrical power, inspection, and maintenance.
- The costs of installing sacrificial systems based on thermally sprayed zinc typically range between 10 and 20 dollars per square foot (about 107 to 215 dollars per square meter). Like the present developmental systems, sacrificial-zinc systems require very little maintenance once they are installed.
- Another type of sacrificial system involves the use of zinc sheet and electrically conductive glue. The costs of installing these systems typically range from 8 to 18 dollars per square foot (about 86 to 194 dollars per square meter). These systems also require very little maintenance after installation. Both this and the preceding sacrificial-zinc system have been said to offer 10-year life expectancy. However, according to NACE, pure zinc coats on concrete structures provide only partial protection because of their low driving voltages. Upon exposure, the zinc can become passivated, such that during dry weather, it does not supply protective current to steel rebar.
- The costs of protecting structures by use of the developmental coating materials have been estimated to range from 5 to 9 dollars per square foot (about 54 to 97 dollars per square meter).

This work was done by Louis G. MacDowell of **Kennedy Space Center** *and Joseph Curran of Dynacs, Inc.*

This invention is owned by NASA, and a patent application has been filed. Inquiries concerning nonexclusive or exclusive license for its commercial development should be addressed to the Technology Programs and Commercialization Office, Kennedy Space Center, (321) 867-8130. Refer to KSC-12049.

Processable Polyimides Containing APB and Reactive End Caps

Properties can be tailored through choice of proportions of dianhydrides and APB.

Langley Research Center, Hampton, Virginia

Imide copolymers that contain 1,3-bis(3-aminophenoxy)benzene (APB) and other diamines and dianhydrides and that are terminated with appropriate amounts of reactive end caps have been invented. The reactive end caps investigated thus far include 4-phenylethynyl phthalic anhydride (PEPA), 3-aminophenoxy-4'-phenylethynylbenzophenone (3-APEB), maleic anhydride (MA), and 5-norbornene-2,3-dicarboxylic anhydride [also known as nadic anhydride (NA)]. The advantage of these copolyimides terminated with reactive groups, relative to other polyimides terminated with reactive groups, is a combination of (1) higher values of desired mechanical-property parameters and (2) greater ease of processing into useful parts.

Homopolymers that contain only other diamines and dianhydrides and that are not processable under conditions reported previously can be made processable by incorporating various amounts of APB according to this invention, depending on the chemical structures of the diamines and dianhydrides used. These copolyimides exhibit high degrees of resistance to solvents, high glass-transition temperatures, and high moduli of elasticity, but are processable at low pressures [≤ 200 psi (≤1.38 MPa)], when the appropriate amounts of APB are utilized. In addition, when these copolymers are terminated with phenylethynyl groups, they exhibit long-term melt stability (several hours at temperatures approaching 300 °C).

The dianhydride incorporated into a polymer of this type has a rigid molecular structure that tends to degrade processability. The addition of the highly flexible APB diamine improves processability, while the imide structure provides stiffness to the polymer backbone, increases resistance to solvents, and improves mechanical properties. The resulting combination of properties is important for the use of the copolymer as a matrix in a composite material or as an adhesive or a film, coating, or molding material: If too little APB is incorporated into the polymer backbone, the resulting material is not processable under desired processing limitations. If too much APB is incorporated into the polymer backbone, the resulting material becomes highly flexible with a lower glass-transition temperature than desired.

Hence, by choosing the ratio between the amount of APB and the amount of the other diamine in the polyimide backbone, one can obtain a material that has a unique combination of solubility, glass-transition temperature, melting temperature, melt viscosity, toughness, and high-temperature mechanical properties. The exact amount of APB needed to optimize this combination of properties is not predictable and must be determined for the intended application and for the proposed method of processing the copolymer for use in the application.

This work was done by Brian J. Jensen of **Langley Research Center**. *Further information is contained in a TSP (see page 1).*

This invention has been patented by NASA (U.S. Patent No. 6,133,401). Inquiries concerning nonexclusive or exclusive license for its commercial development should be addressed to Greg Manuel, Technology Commercialization Program Office, Langley Research Center, MS 200, Hampton, VA 23861, g.s.manuel@larc.nasa.gov. Refer to LAR-15449.

Rod/Coil Block Copolyimides for Ion-Conducting Membranes

Lithium cells and fuel cells could function over wider temperature ranges.

John H. Glenn Research Center, Cleveland, Ohio

Rod/coil block copolyimides that exhibit high levels of ionic conduction can be made into diverse products, including dimensionally stable solid electrolyte membranes that function well over wide temperature ranges in fuel cells and in lithium-ion electrochemical cells. These rod/coil block copolyimides were invented to overcome the limitations of polymers now used to make such membranes. They could also be useful in other electrochemical and perhaps some optical applications, as described below.

The membranes of amorphous polyethylene oxide (PEO) now used in lithium-ion cells have acceptably large ionic conductivities only at temperatures above 60 °C, precluding use in what would otherwise be many potential applications at lower temperatures. PEO is difficult to process, and, except at the highest molecular weights it is not very dimensionally stable.

It would be desirable to operate fuel cells at temperatures above 80 °C to take advantage of better kinetics of redox reactions and to reduce contamination of catalysts. Unfortunately, proton-conduction performance of a typical perfluorosulfonic polymer membrane now used as a solid electrolyte in a fuel cell decreases with increasing temperature above 80 °C because of loss of water from within the membrane. The loss of water has been attributed to the hydrophobic nature of the polymer backbone. In addition, perfluorosulfonic polymers are expensive and are not sufficiently stable for long-term use.

Rod/coil block copolyimides are so named because each molecule of such a polymer comprises short polyimide rod segments alternating with flexible polyether coil segments (see figure). The rods and coils can be linear, branched, or mixtures of linear and branched. A unique feature of these polymers is that the rods and coils are highly incompatible, giving rise to a phase separation with a high degree of ordering that creates nanoscale channels in which ions can travel freely. The conduction of ions can occur in the coil phase, the rod phase, or both phases. The rod phase also imparts dimensional and mechanical stability to the polymer. In the case of a rod/coil block copolyimide synthesized for use in a fuel cell, the incorporation of the polyether coils enables the polymer to hold water at higher temperatures than it could in the absence of these coils.

Rod/coil block copolyimides can be synthesized and processed easily (e.g., by solution casting) to make membranes. These polymers are expected to cost less than perfluorosulfonic polymers. Suitable functionality can be introduced into the rods and/or coils to produce or enhance (1) retention of water; (2) the transport of lithium ions in a lithium-ion cell; (3) the transport of protons for use in a fuel cell; (4) the transport of the aforementioned or other ions for use in chemical sensors, ion sensors, water-purification devices, and other electrochemical devices; and/or (5) optical properties for use in optical waveguides.

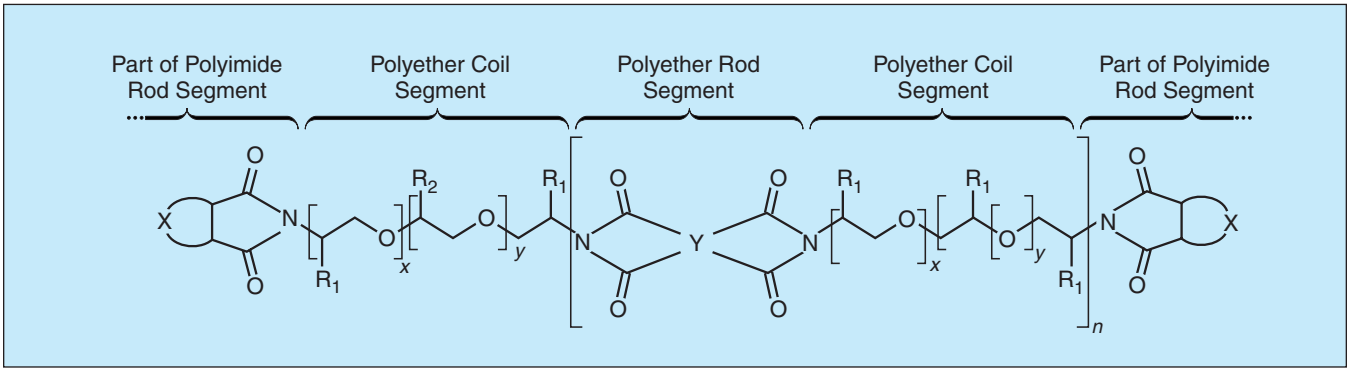

A **Rod/Coil Block Copolyimide** molecule comprises polyether coil segments and polyimide rod segments. R_1 denotes a hydrogen, alkyl, or alkoxy radical; R_2 denotes hydrogen or an alkyl or alkoxy group and may be the same as, or different from, R_1; X denotes an aromatic or aliphatic group; Y denotes any of a variety of straight or branched polyimide segments; *x* and *y* are zero or greater; and *n* is 1 or greater.

This work was done by Mary Ann B. Meador and James D. Kinder of **Glenn Research Center**. *Further information is contained in a TSP (see page 1).*

Inquiries concerning rights for the commercial use of this invention should be addressed to NASA Glenn Research Center, Commercial Technology Office, Attn: Steve Fedor, Mail Stop 4–8, 21000 Brookpark Road, Cleveland, Ohio 44135. Refer to LEW-17299.

Techniques for Characterizing Microwave Printed Antennas

Slot-line and other printed antennas can be characterized quickly and inexpensively.

John H. Glenn Research Center, Cleveland, Ohio

The combination of a de-embedding technique and a direct on-substrate measurement technique has been devised to enable measurement of the electrical characteristics (impedances, scattering parameters, and gains) of microwave printed antennas that may be formed integrally with feed networks that include slot lines, coplanar striplines, and/or coplanar waveguides. The combination of techniques eliminates the need for custom test fixtures, including transitions between (1) coaxial or waveguide feed lines in typical test equipment and (2) the planar waveguide structures of the printed circuits under test. The combination of techniques can be expected to be especially useful for rapid, inexpensive, and accurate characterization of antennas for miniature wireless communication units that operate at frequencies from a few to tens of gigahertz.

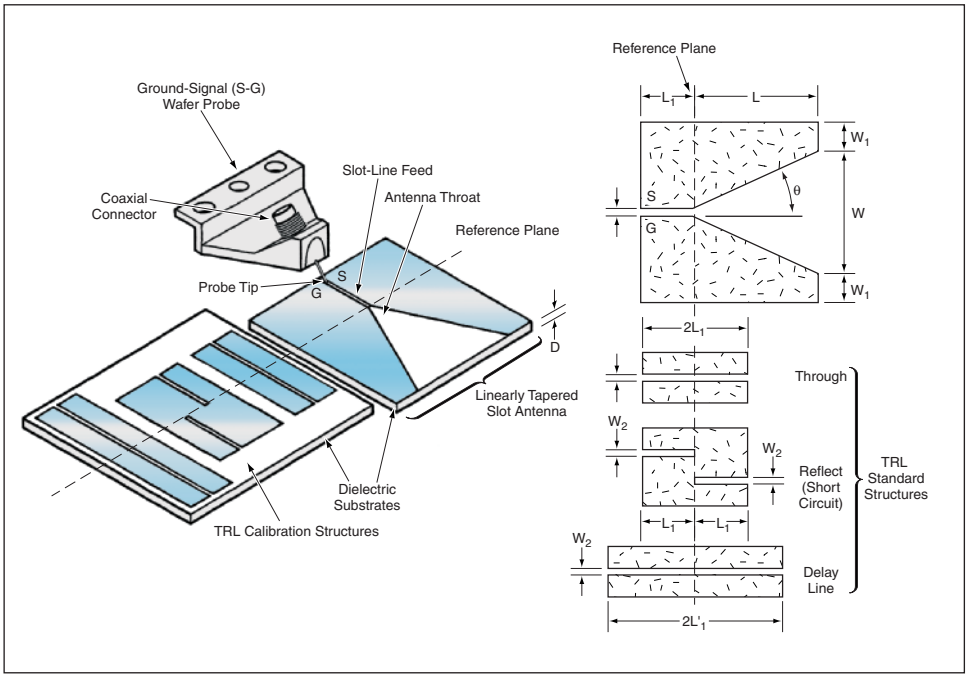

Figure 1. **Measurements at the Input Terminals** of the slot-line feed of a linearly tapered slot-line antenna are referred to a plane at the antenna throat (the narrow end of the taper) by means of (a) calibration measurements on TRL standard structures and (b) de-embedding software.

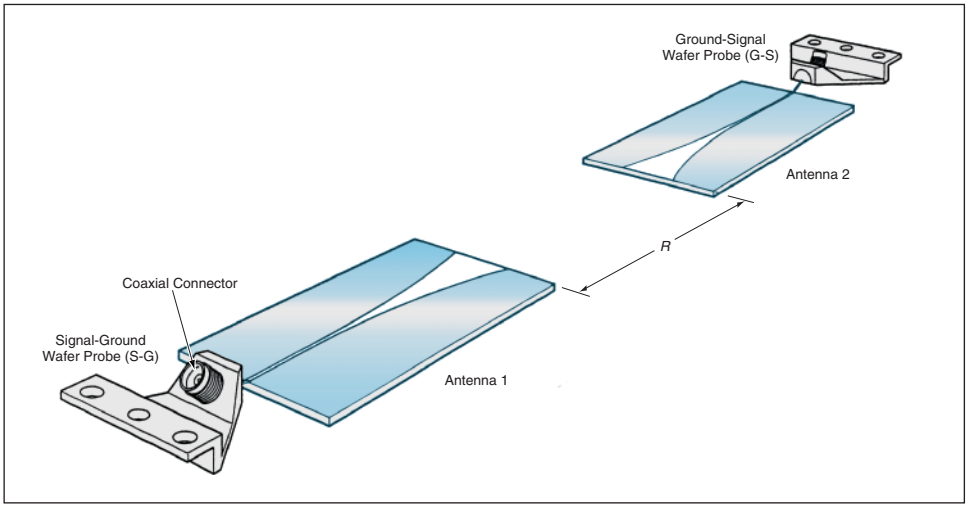

Figure 2. The **Gain of Two Identical Vivaldi Antennas** (exponentially tapered slot-line antennas) can be measured by the direct on-substrate measurement technique and this geometric arrangement. The distance *R* must be made large enough that far-field conditions prevail.

Both techniques involve the use of an automatic network analyzer (ANA) coupled with a wafer probe station and a pair of ground-signal microwave probes. The de-embedding technique includes the established through-reflect-line (TRL) calibration technique, which involves the fabrication and testing of standard calibration structures on the same substrate alongside an antenna that one seeks to characterize (for example, see Figure 1). The dimensions of the calibration structures are related to those of the antenna in a predetermined way. For the TRL measurements, the ANA is operated under the control of de-embedding software developed by the National Institute of Standards and Technology (NIST). This software processes the TRL measurement data to establish an electrical reference plane in the antenna, to which plane all de-embedded scattering parameters and impedances are meant to be referred. Thereafter, the de-embedding software can be used to obtain the reference-plane characteristics of the antenna from ANA measurements taken at the input terminals of the slot-line feed.

The direct on-substrate measurement technique involves the calibration of the ground-signal microwave probes to their tips. This calibration is done by use of the ANA with an open circuit, a short circuit, and a matched load as standards. The stan-

dards for direct measurements are provided by the probe manufacturer on an impedance standard substrate. Calibrated probes are then put in contact with the input terminals of the slot-line feed of the antenna, and the antenna is excited via the probes. The direct on-substrate measurement technique is best suited for designs in which the slot-line feeds are short enough to interfere only minimally with the probes.

Figure 2 depicts a setup for measuring the absolute gain of a pair of identical antennas. In this case, the antenna input and output measurements are made by the direct on-substrate probe measurement technique, the antennas are oriented facing each other and matched in polarization, and the antennas are placed far enough apart that, to a close approximation, far-field radiation conditions prevail. The gain is calculated from the geometric parameters of the setup, and from the transmitted and received power levels measured by the ANA via the probes connected to the terminals of the transmitting and receiving antennas, respectively.

This work was done by Rainee Simons of NYMA/Federal Data Corp. and Richard Q. Lee of **Glenn Research Center**. *Further information is contained in a TSP (see page 1).*

Inquiries concerning rights for the commercial use of this invention should be addressed to NASA Glenn Research Center, Commercial Technology Office, Attn: Steve Fedor, Mail Stop 4–8, 21000 Brookpark Road, Cleveland, Ohio 44135. Refer to LEW-17040.

Cylindrical Antenna With Partly Adaptive Phased-Array Feed

The cost of a high-performance antenna could be reduced.

NASA's Jet Propulsion Laboratory, Pasadena, California

A proposed design for a phased-array-fed cylindrical-reflector microwave antenna would enable enhancement of the radiation pattern through partially adaptive amplitude and phase control of its edge radiating feed elements. Antennas based on this design concept would be attractive for use in radar (especially synthetic-aperture radar) and other systems that could exploit electronic directional scanning and in which there are requirements for specially shaped radiation patterns, including ones with low side lobes. One notable advantage of this design concept is that the transmitter/receiver modules feeding all the elements except the edge ones could be identical and, as a result, the antenna would cost less than in the cases of prior design concepts in which these elements may not be identical.

The basic antenna geometry (see figure) is that of a parabolic cylindrical reflector. The cylindrical axis is the y axis, and the geometric boresight axis is the z axis. The phased array of feed elements lies on the focal line, which is parallel to the y axis, at a distance F from the apex of the parabola. The boundary of the reflector and thus of the aperture, as projected onto the x,y plane, is specified by the superquadric curve

$$\left|\frac{x}{a}\right|^m + \left|\frac{y}{b}\right|^m = 1$$

where a and b are the lengths of the x and y semiaxes, respectively, of the aperture; and m is a parameter that can be chosen to control the rounded shape of the corners. These basic geometric characteristics are the same as those of the antenna described in "Low-Sidelobe Phased-Array-Fed Cylindrical-Reflector Antenna (NPO-20494), *NASA Tech Briefs*, Vol. 24, No. 2 (February 2000), page 5a.

For the non-edge radiating elements, the amplitudes may be chosen to obtain suitably shaped main and side lobes, and the phase difference between adjacent elements would be set at the value needed to point the main lobe in the desired direction. For the nth non-edge element, the excitation coefficient would be of the form

$$a_n e^{jn\alpha},$$

where a_n is the magnitude of the excitation, and α is the progressive phase

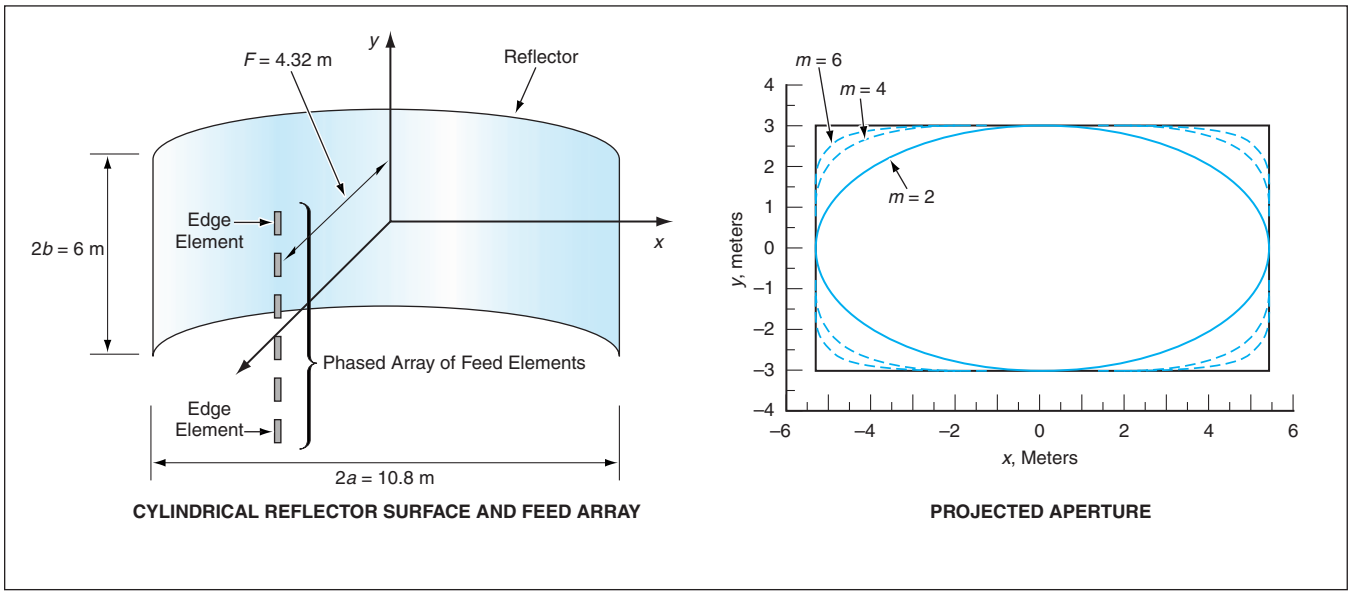

Figure 1. In an **Antenna With a Phased-Array Feed and a Parabolic Cylindrical Reflector** the amplitudes and phases of excitation of the edge elements can be chosen differently from those of the other radiating elements to reduce or cancel side lobes of the radiation pattern.

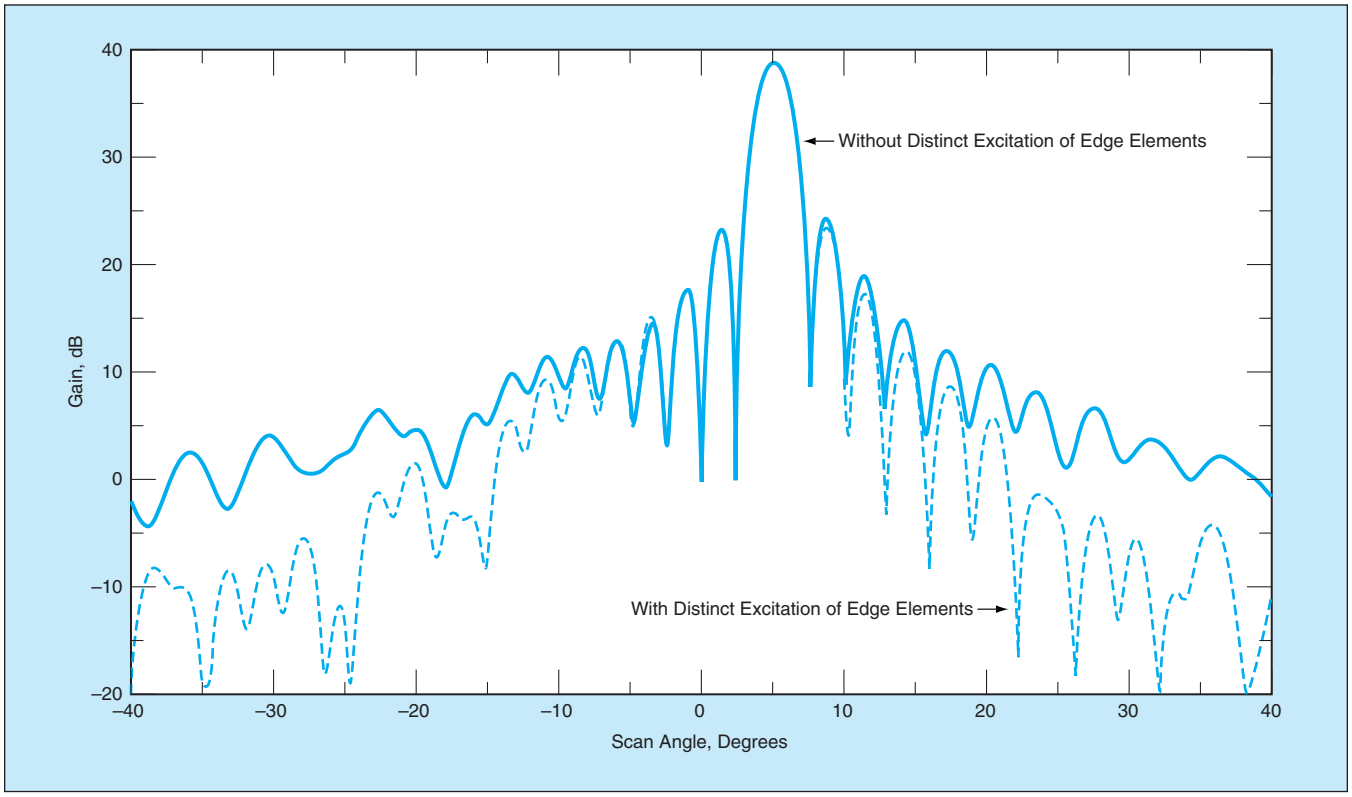

Figure 2. **Results of Numerical Simulations,** with and without distinct excitation of the edge elements, are plotted for a scan angle of 5°.

(that is, the phase difference between adjacent elements) needed to point the main lobe of the radiation beam in a given direction in the (y,z) plane. For an edge radiating element, the excitation coefficient would be of the form

$$we^{j\phi} = a_{\pm N/2}e^{\pm jN\alpha/2}(1+ce^{\pm j\delta}),$$

where w and $a_{\pm N/2}$ are magnitudes; ϕ is the phase of the excitation; c and δ are a magnitude scale factor and a phase shift, respectively, necessary for the desired degree of cancellation of a specified side lobe, and N is one less than the total number of radiating elements.

Computational simulations have been performed, following diffraction-analysis procedures based on a physical-optics formulation. Some of the parameters used in the simulations were $a = 5.4$ m, $b = 3$ m, $F = 4.32$ m, and $N + 1$ (the number of elements) = 41. The phased array had a length equal to that of the cylindrical axis of the antenna ($2b = 6$ m) and comprised 41 y-polarized elements spaced at intervals of 0.63 wavelength. The results of the computational simulations showed that the radiation pattern could be controlled with high versatility through control of the edge-element excitation amplitudes and phases. In particular, it was demonstrated that the side-lobe levels could be reduced (see Figure 2) and even effectively canceled and that side-lobe envelopes could be made steeper (side-lobe levels made lower) by choosing, for cancellation, a specific side lobe near the peak of the main lobe. In addition, one could choose the edge-element excitations to obtain different side-lobe envelopes simultaneously on the opposite sides of the main lobe.

This work was done by Ziad Hussein and Jeff Hilland of Caltech for **NASA's Jet Propulsion Laboratory**. *Further information is contained in a TSP (see page 1).*
NPO-30251

Command Interface ASIC — Analog Interface ASIC Chip Set

These are radiation-hard integrated circuits for power-control applications.

NASA's Jet Propulsion Laboratory, Pasadena, California

A command interface application-specific integrated circuit (ASIC) and an analog interface ASIC have been developed as a chip set for remote actuation and monitoring of a collection of switches, which can be used to control generic loads, pyrotechnic devices, and valves in a high-radiation environment. The command interface ASIC (CIA) can be used alone or in combination with the analog interface ASIC (AIA). Designed primarily for incorporation into spacecraft control systems, they are also suitable for use in high-radiation terrestrial environments (e.g., in nuclear power plants and facilities that process radioactive materials).

The primary role of the CIA within a spacecraft or other power system is to provide a reconfigurable means of regulating the power bus, actuating all valves, firing all pyrotechnic devices, and controlling the switching of power to all switchable loads. The CIA is a mixed-signal (analog and digital) ASIC that includes an embedded microcontroller with supporting fault-tolerant switch-control and monitoring circuitry that is

capable of connecting to a redundant set of interintegrated circuit (I^2C) buses. Commands and telemetry requests are communicated to the CIA. Adherence to the I^2C bus standard helps to reduce development costs by facilitating the use of previously developed, commercially available components.

The AIA is a mixed-signal ASIC that includes the analog circuitry needed to connect the CIA to a custom higher-powered version of the I^2C bus. The higher-powered version is designed to enable operation with bus cables longer than those contemplated in the I^2C standard. If there are multiple higher-power I^2C-like buses, then there must an AIA between the CIA and each such bus. The AIA includes two identical interface blocks: one for the side-A I^2C clock and data buses and the other for the side B buses. All the AIAs on each side are powered from a common power converter module (PCM). Sides A and B of the I^2C buses are electrically isolated from each other (see figure). They are also isolated from the CIA by use of transformer coupling of signals between the AIA blocks and the CIA.

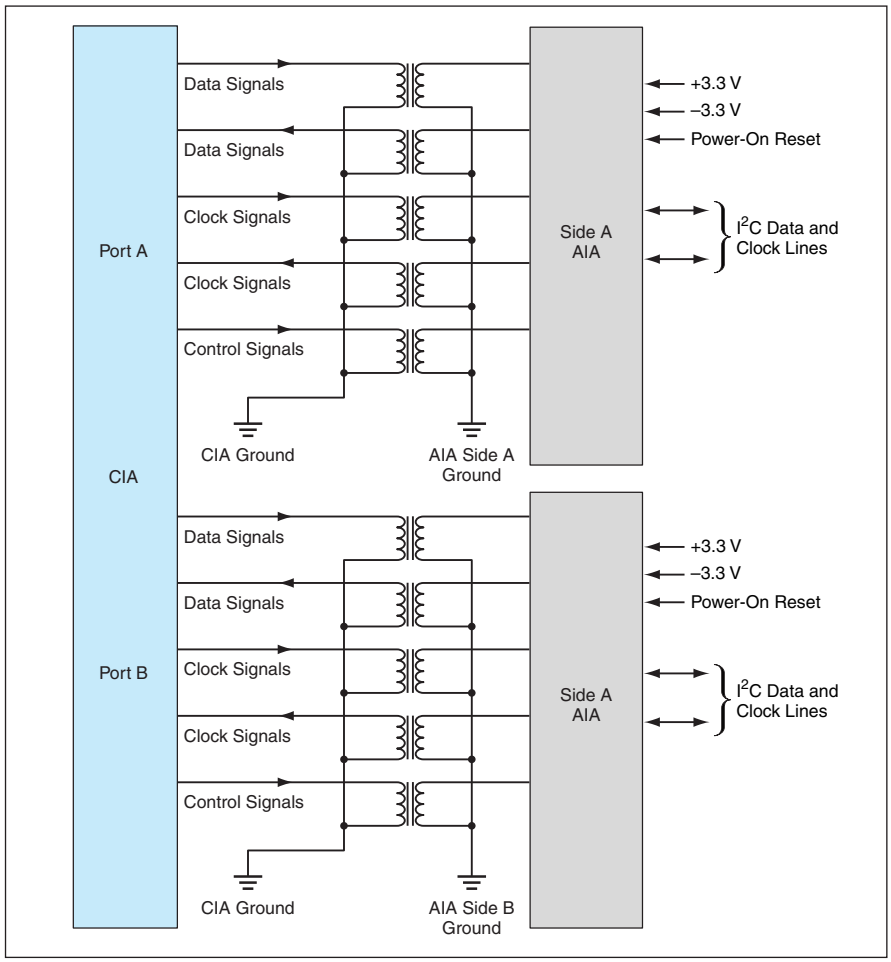

The **AIA and the Interface between the AIA and the CIA** provide ground isolation between the CIA and sides A and B of the I^2C bus.

This work was done by Baldes Ruiz, Burton Jaffe, Gary Burke, Gerald Lung, Gregory Pixler, Joe Plummer, Sunant Katanyoutanant, and William Whitaker of Caltech for **NASA's Jet Propulsion Laboratory**. *Further information is contained in a TSP (see page 1).*

In accordance with Public Law 96-517, the contractor has elected to retain title to this invention. Inquiries concerning rights for its commercial use should be addressed to:

Intellectual Assets Office
JPL
Mail Stop 202-233
4800 Oak Grove Drive
Pasadena, CA 91109
(818) 354-2240
E-mail: ipgroup@jpl.nasa.gov

Refer to NPO-30275, volume and number of this NASA Tech Briefs *issue, and the page number.*

Predicting Accumulations of Ice on Aerodynamic Surfaces

LEWICE is a computer program that predicts the accumulation of ice on two-dimensional aerodynamic surfaces under conditions representative of the flight of an aircraft through an icing cloud. The software first calculates the airflow surrounding the body of interest, then uses the airflow to compute the trajectories of water droplets that impinge on the surface of the body. The droplet trajectories are also used to compute impingement limits and local collection efficiencies, which are used in subsequent ice-growth calculations and are also useful for designing systems to protect against icing. Next, the software predicts the shape of accumulating ice by modeling transfers of mass and energy in small control volumes. The foregoing computations are repeated over several computational time steps until the total icing exposure time is reached. Results of computations by LEWICE have been compared with an extensive database of measured ice shapes obtained from experiments, and have been shown to closely approximate those shapes under most conditions of interest to the aviation community.

This program was written by Colin Bidwell, Mark Potapczuk, and Gene Addy of **Glenn Research Center** *and William Wright of QSS Group, Inc. Further information is contained in a TSP (see page 1).*

Inquiries concerning rights for the commercial use of this invention should be addressed to NASA Glenn Research Center, Commercial Technology Office, Attn: Steve Fedor, Mail Stop 4-8, 21000 Brookpark Road, Cleveland Ohio 44135. Refer to LEW-17378.

Analyzing Aeroelasticity in Turbomachines

ASTROP2-LE is a computer program that predicts flutter and forced responses of blades, vanes, and other components of such turbomachines as fans, compressors, and turbines. ASTROP2-LE is based on the ASTROP2 program, developed previously for analysis of stability of turbomachinery components. In developing ASTROP2-LE, ASTROP2 was modified to include a capability for modeling forced responses. The program was also modified to add a capability for analysis of aeroelasticity with mistuning and unsteady aerodynamic solutions from another program, LINFLX2D, that solves the linearized Euler equations of unsteady two-dimensional flow. Using LINFLX2D to calculate unsteady aerodynamic loads, it is possible to analyze effects of transonic flow on flutter and forced response. ASTROP2-LE can be used to analyze subsonic, transonic, and supersonic aerodynamics and structural mistuning for rotors with blades of differing structural properties. It calculates the aerodynamic damping of a blade system operating in airflow so that stability can be assessed. The code also predicts the magnitudes and frequencies of the unsteady aerodynamic forces on the airfoils of a blade row from incoming wakes. This information can be used in high-cycle-fatigue analysis to predict the fatigue lives of the blades.

This program was written by O. Mehmed of **Glenn Research Center** *and T. S. R. Reddy and R. Srivastava of the University of Toledo. Further information is contained in a TSP (see page 1).*

Inquiries concerning rights for the commercial use of this invention should be addressed to NASA Glenn Research Center, Commercial Technology Office, Attn: Steve Fedor, Mail Stop 4-8, 21000 Brookpark Road, Cleveland Ohio 44135. Refer to LEW-17477.

Software for Allocating Resources in the Deep Space Network

TIGRAS 2.0 is a computer program designed to satisfy a need for improved means for analyzing the tracking demands of interplanetary space-flight missions upon the set of ground antenna resources of the Deep Space Network (DSN) and for allocating those resources. Written in Microsoft Visual C++, TIGRAS 2.0 provides a single rich graphical analysis environment for use by diverse DSN personnel, by connecting to various data sources (relational databases or files) based on the stages of the analyses being performed. Notable among the algorithms implemented by TIGRAS 2.0 are a DSN antenna-load-forecasting algorithm and a conflict-aware DSN schedule-generating algorithm. Computers running TIGRAS 2.0 can also be connected using SOAP/XML to a Web services server that provides analysis services via the World Wide Web. TIGRAS 2.0 supports multiple windows and multiple panes in each window for users to view and use information, all in the same environment, to eliminate repeated switching among various application programs and Web pages. TIGRAS 2.0 enables the use of multiple windows for various requirements, trajectory-based time intervals during which spacecraft are viewable, ground resources, forecasts, and schedules. Each window includes a time navigation pane, a selection pane, a graphical display pane, a list pane, and a statistics pane.

This program was written by Yeou-Fang Wang, Chester Borden, Silvino Zendejas, and John Baldwin of Caltech for **NASA's Jet Propulsion Laboratory**. *Further information is contained in a TSP (see page 1).*

This software is available for commercial licensing. Please contact Don Hart of the California Institute of Technology at (818) 393-3425. Refer to NPO-30856.

Expert Seeker

Expert Seeker is a computer program of the knowledge-management-system (KMS) type that falls within the category of expertise-locator systems. The main goal of the KMS system implemented by Expert Seeker is to organize and distribute knowledge of who are the domain experts within and without a given institution, company, or other organization. The intent in developing this KMS was to enable the re-use of organizational knowledge and provide a methodology for querying existing information (including structured, semistructured, and unstructured information) in a way that could help identify organizational experts. More specifically, Expert Seeker was developed to make it possible, by use of an intranet, to do any or all of the following:

- Assist an employee in identifying who has the skills needed for specific projects and to determine whether the experts so identified are available.
- Assist managers in identifying employees who may need training opportunities.
- Assist managers in determining what

expertise is lost when employees retire or otherwise leave.
- Facilitate the development of new ways of identifying opportunities for innovation and minimization of duplicated efforts.
- Assist employees in achieving competitive advantages through the application of knowledge-management concepts and related systems.
- Assist external organizations in requesting speakers for specific engagements or determining from whom they might be able to request help via electronic mail.
- Help foster an environment of collaboration for rapid development in today's environment, in which it is increasingly necessary to assemble teams of experts from government, universities, research laboratories, and industries, to quickly solve problems anytime, anywhere.
- Make experts more visible.
- Provide a central repository of information about employees, including information that, heretofore, has typically not been captured by the human-resources systems (e.g., information about past projects, patents, or hobbies).
- Unify myriad collections of data into Web-enabled repository that could easily be searched for relevant data.

This program was written by Irma Becerra Fernandez of Florida International University for **Kennedy Space Center.** *For further information, contact the Kennedy Commercial Technology Office at (321) 867-8130. KSC-12498*

High-Speed Recording of Test Data on Hard Disks

Disk Recording System (DRS) is a systems-integration computer program for a direct-to-disk (DTD) high-speed data-acquisition system (HDAS) that records rocket-engine test data. The HDAS consists partly of equipment originally designed for recording the data on tapes. The tape recorders were replaced with hard-disk drives, necessitating the development of DRS to provide an operating environment that ties two computers, a set of five DTD recorders, and signal-processing circuits from the original tape-recording version of the HDAS into one working system. DRS includes three subsystems: (1) one that generates a graphical user interface (GUI), on one of the computers, that serves as a main control panel; (2) one that generates a GUI, on the other computer, that serves as a remote control panel; and (3) a data-processing subsystem that performs tasks on the DTD recorders according to instructions sent from the main control panel. The software affords capabilities for dynamic configuration to record single or multiple channels from a remote source, remote starting and stopping of the recorders, indexing to prevent overwriting of data, and production of filtered frequency data from an original time-series data file.

This program was written by Paul M. Lagarde, Jr., of the Boeing Co. and Bruce Newnan of Integrated System Consultants for **Stennis Space Center**.

Inquiries concerning rights for the commercial use of this invention should be addressed to the Intellectual Property Manager, Stennis Space Center, (228) 688-1929. Refer to SSC-00188.

Functionally Graded Nanophase Beryllium/Carbon Composites

The main advantage, relative to Co/WC/diamond composites, is less weight.

Lyndon B. Johnson Space Center, Houston, Texas

Beryllium, beryllium alloys, beryllium carbide, and carbon are the ingredients of a class of nanophase Be/Be_2C/C composite materials that can be formulated and functionally graded to suit a variety of applications. In a typical case, such a composite consists of a first layer of either pure beryllium or a beryllium alloy, a second layer of B_2C, and a third layer of nanophase sintered carbon derived from fullerenes and nanotubes. The three layers are interconnected through interpenetrating spongelike structures.

These Be/Be_2C/C composite materials are similar to Co/WC/diamond functionally graded composite materials, except that (1) W and Co are replaced by Be and alloys thereof and (2) diamond is replaced by sintered carbon derived from fullerenes and nanotubes. (Optionally, one could form a Be/Be_2C/diamond composite.) Because Be is lighter than W and Co, the present Be/Be_2C/C composites weigh less than do the corresponding Co/WC/diamond composites. The nanophase carbon is almost as hard as diamond.

WC/Co is the toughest material. It is widely used for drilling, digging, and machining. However, the fact that W is a heavy element (that is, has high atomic mass and mass density) makes W unattractive for applications in which weight is a severe disadvantage. Be is the lightest tough element, but its toughness is less than that of WC/Co alloy. Be strengthened by nanophase carbon is much tougher than pure or alloy Be. The nanophase carbon has an unsurpassed strength-to-weight ratio.

The Be/Be_2C/C composite materials are especially attractive for terrestrial and aerospace applications in which there are requirements for light weight along with the high strength and toughness of the denser Co/WC/diamond materials. These materials could be incorporated into diverse components, including cutting tools, bearings, rocket nozzles, and shields. Moreover, because Be and C are effective as neutron moderators, Be/Be_2C/C composites could be attractive for some nuclear applications.

This work was done by Oleg A. Voronov and Gary S. Tompa of Diamond Materials Inc. for **Johnson Space Center**. *Further information is contained in a TSP (see page 1).*
MSC-23274

Thin Thermal-Insulation Blankets for Very High Temperatures

One blanket would have about the thickness of several sheets of paper.

Goddard Space Flight Center, Greenbelt, Maryland

Thermal-insulation blankets of a proposed type would be exceptionally thin and would endure temperatures up to 2,100 °C. These blankets were originally intended to protect components of the NASA Solar Probe spacecraft against radiant heating at its planned closest approach to the Sun (a distance of 4 solar radii). These blankets could also be used on Earth to provide thermal protection in special applications (especially in vacuum chambers) for which conventional thermal-insulation blankets would be too thick or would not perform adequately.

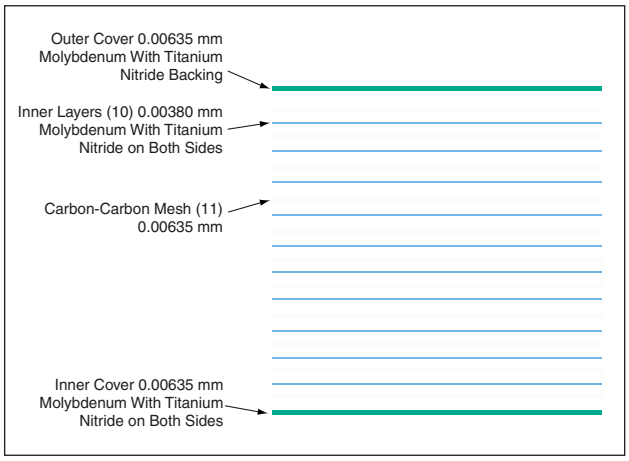

This **Thermal-Insulation Blanket** would be very thin and lightweight. The blanket would be made of materials that melt at temperatures greater than 2,100 °C.

A blanket according to the proposal (see figure) would be made of molybdenum, titanium nitride, and carbon-carbon composite mesh, which melt at temperatures of 2,610, 2,930, and 2,130 °C, respectively. The emittance of molybdenum is 0.24, while that of titanium nitride is 0.03. Carbon-carbon composite mesh is a thermal insulator.

Typically, the blanket would include 0.25-mil (≈0.00635-mm)-thick hot-side and cold-side cover layers of molybdenum. Titanium nitride would be vapor-deposited on both surfaces of each cover layer. Between the cover layers there would be 10 inner layers of 0.15-mil (≈0.0038-mm)-thick molybdenum with vapor-deposited titanium nitride on both sides of each layer. The thickness of each titanium nitride coat would be about 1,000 Å. The cover and inner layers would be interspersed with 0.25-mil (0.00635-mm)-thick layers of carbon-carbon composite mesh. The blanket would have total thickness of 4.75 mils (≈0.121 mm) and an areal mass density of 0.7 kg/m^2. One could, of course, increase the thermal-insulation capability of the blanket by increasing number of inner layers (thereby unavoidably increasing the total thickness and mass density).

This work was done by Michael K. Choi of **Goddard Space Flight Center.** *Further information is contained in a TSP (see page 1).*
GSC-14386

Aerostructures Test Wing

Test data can be used to refine predictions of the onset of flutter.

Dryden Flight Research Center, Edwards, California

The Aerostructures Test Wing (ATW) was an apparatus used in a flight experiment during a program of research on aeroelastic instabilities. The ATW experiment was performed to study a specific instability known as flutter. Flutter is a destructive phenomenon caused by adverse coupling of structural dynamics and aerodynamics. The process of determining a flight envelope within which an aircraft will not experience flutter, known as flight flutter testing, is very dangerous and expensive because predictions of the instability are often unreliable.

The ATW was a small-scale airplane wing that comprised an airfoil and boom (see upper part of Figure 1). For flight tests, the ATW was mounted on the F-15B/FTF-II testbed, which is a second-generation flight-test fixture described in "Flight-Test Fixture for Aerodynamic Research" (DRC-95-27), *NASA Tech Briefs*, Vol. 19, No. 9, September 1995, page 84. The ATW was mounted horizontally on this fixture, and the entire assembly was attached to the undercarriage of the F-15B airplane (see lower part of Figure 1).

The primary objective of the ATW project was to investigate traditional and advanced methodologies for predicting the onset of flutter. In particular, the ATW generated data that were used to evaluate a flutterometer. This particular flutterometer is an on-line computer program that uses μ-method analysis to estimate worst-case flight conditions associated with flutter. This software was described in "A Flutterometer Flight Test Tool" *NASA Tech Briefs*, Vol. 23, No. 1, January 1999, page 52.

Flutter predictions can be evaluated only by comparison with measured flight conditions at which flutter was encountered. Therefore, the ATW was designed to enable the safe observation of the flutter instability. It was essential to ensure that the destruction of the ATW did not cause any damage to the host F-15B airplane. The ATW was constructed out of fiberglass, composite, and foam. Hence, the entire ATW was lightweight and frangible, so any pieces that struck the F-15 airplane would exert only minimal effects and would cause no damage.

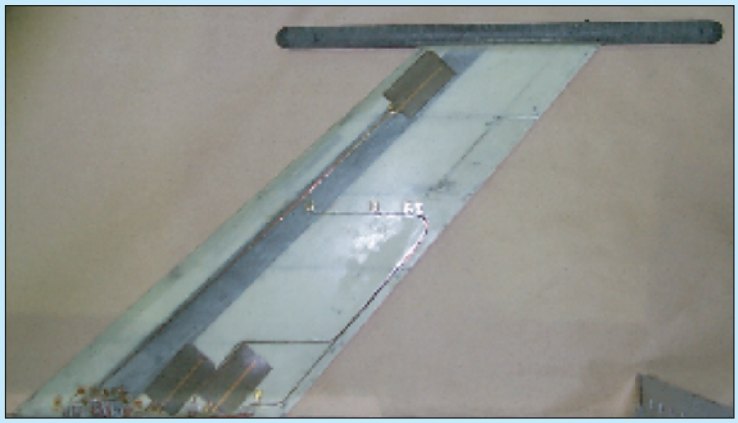

AEROSTRUCTURES TEST WING (TOP VIEW)

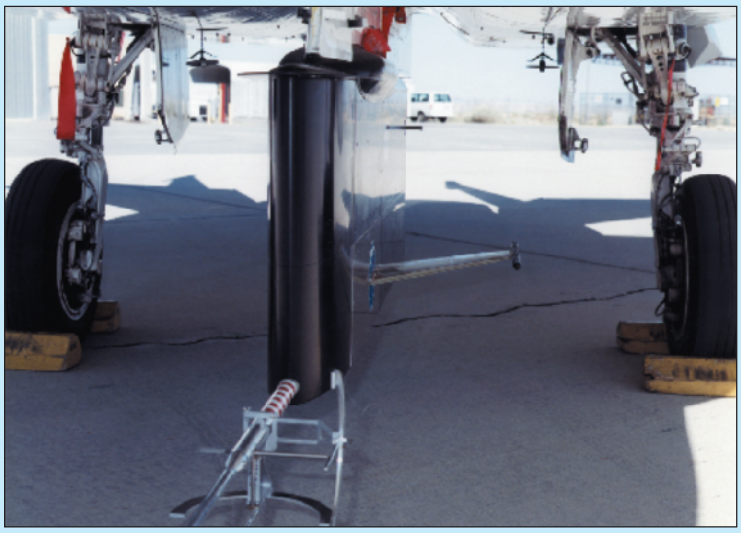

AEROSTRUCTURES TEST WING MOUNTED ON THE F-15B-FTF-11

Figure 1. The **Aerostructures Test Wing** was a small-scale airplane wing that was subjected to flight tests to investigate flutter and related phenomena.

It was also important to ensure that the ATW could generate data that are sufficient for the flutterometer and other means of flutter prediction. This requirement was satisfied by incorporating an excitation and measurement system into the ATW. The excitation was provided by commanding frequency-varying sweeps of energy through a set of piezoelectric patches on the surface of the wing. The measurements were provided by strain gauges throughout the wing and accelerometers in the boom.

The first phase of the ATW program was pre-flight ground testing. This testing was performed in consideration of both static and dynamic properties of the ATW. Deflection tests were performed to determine the sizes of static loads that could be borne by the ATW. Vibration tests were also performed to determine the dynamic modal characteristics of the ATW. It was shown that the first bending and torsion modes were at frequencies of 14.05 and 22.38 Hz. The data from these tests were

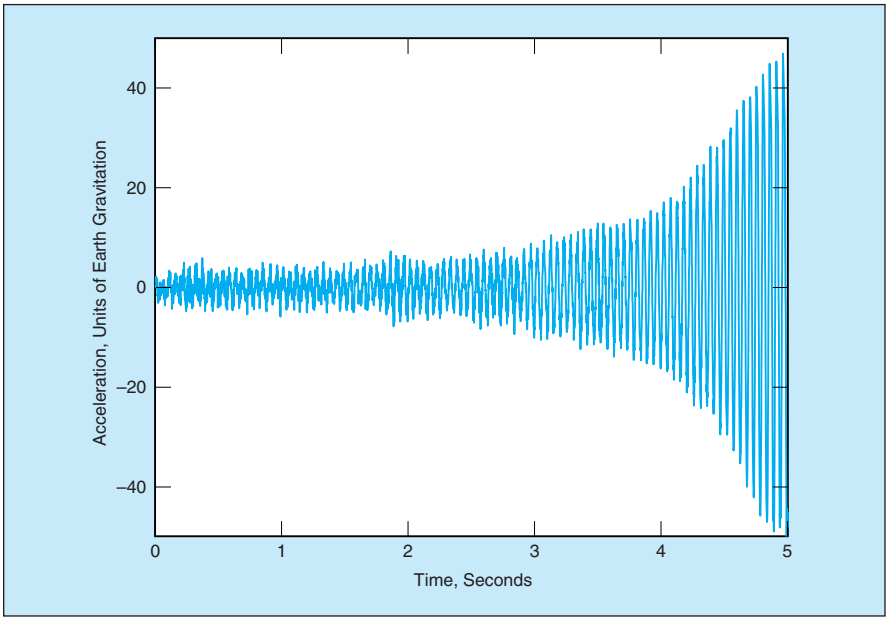

Figure 2. This **Accelerometer Response** shows the onset of flutter.

used to generate computational models for predicting the onset of flutter.

The second phase of the ATW program was a flight test for envelope expansion. In this phase, it was required to analyze experimental data acquired at a series of test points with increasing velocity and dynamic pressure. At each test point, the ATW was excited with a frequency-varying input and its responses were measured by sensors. The resulting flight data were telemetered to a control room and analyzed by the flutter-prediction methodologies. A total of five flight tests were performed in April 2001.

A flutter instability of the ATW was encountered at approximately mach 0.83 at an altitude 10,000 feet (≈3 km). The wing was broken such that the boom and roughly 30 percent of the wing were lost. The pieces fell to the ground without striking the F-15B aircraft or FTF-II testbed. The flutter incident was quite demonstrative of the phenomenon. The instability was encountered during a slow acceleration from mach 0.825 to mach 0.830. The damping changed dramatically during this acceleration. The ATW went from stable, with accelerometer responses going from approximately 3 *g* (where *g* = the standard gravitational acceleration at the surface of the Earth) to unstable during a time interval of only 5 seconds (see Figure 2).

The data from the ATW were analyzed to evaluate the flutter-prediction methodologies. The results indicated that computational models were able to predict the onset of flutter reasonably well, but that small errors in the models could cause large errors in the predictions. The traditional approaches for analyzing flight data were shown to afford a capability to predict the onset of flutter only during operation at flight conditions near the instability. The flutterometer was shown to be somewhat conservative in the worst-case estimates of flutter, but it presented a reasonable prediction of flutter at flight conditions that were far from the instability.

This work was done by Rick Lind, David F. Voracek, Tim Doyle, Roger Truax, Starr Potter, Marty Brenner, Len Voelker, and Larry Freudinger of **Dryden Flight Research Center** *and Cliff Sticht of Ames Research Center. For further information, contact the Dryden Commercial Technology Office at (661) 276-3689.*
DRC-01-37

Flight-Test Evaluation of Flutter-Prediction Methods

Experiments have demonstrated the accuracy of predictions of instability.

Dryden Flight Research Center, Edwards, California

The flight-test community routinely spends considerable time and money to determine a range of flight conditions, called a flight envelope, within which an aircraft is safe to fly. The cost of determining a flight envelope could be greatly reduced if there were a method of safely and accurately predicting the speed associated with the onset of an instability called flutter.

Several methods have been developed with the goal of predicting flutter speeds to improve the efficiency of flight testing. These methods include (1) data-based methods, in which one relies entirely on information obtained from the flight tests and (2) model-based approaches, in which one relies on a combination of flight data and theoretical models. The data-driven methods include one based on extrapolation of damping trends, one that involves an envelope function, one that involves the Zimmerman-Weissenburger flutter margin, and one that involves a discrete-time auto-regressive model. An example of a model-based approach is that of the flutterometer. These methods have all been shown to be theoretically valid and have been demonstrated on simple test cases; however, until now, they have not been thoroughly evaluated in flight tests.

An experimental apparatus called the Aerostructures Test Wing (ATW) was developed to test these prediction methods. [The ATW is described in the immediatlely preceding article, "Aerostructures Test Wing" (DRC-01-37)]. The ATW is a small wing-and-boom assembly that has a complicated and realistic structure similar to that of a full-scale airplane wing. The ATW was flown by use of an F-15 airplane and an associated flight-test fixture. The ATW was mounted horizontally on the fixture and the resulting system was attached to the undercarriage of the F-15 fuselage, as shown in preceding article.

For a flight test of flutter-prediction methods, the ATW was flown on four occasions during April 2001. The flight test involved measuring accelerometer responses as a series of test points. The airspeeds of these test points were increased until the onset of flutter was encountered at 460 knots of equivalent airspeed (KEAS) [≈237 m/s equivalent airspeed].

Predictions of the speed associated with flutter were computed at every test point. In each instance, the prediction was based on data from the current test point and any

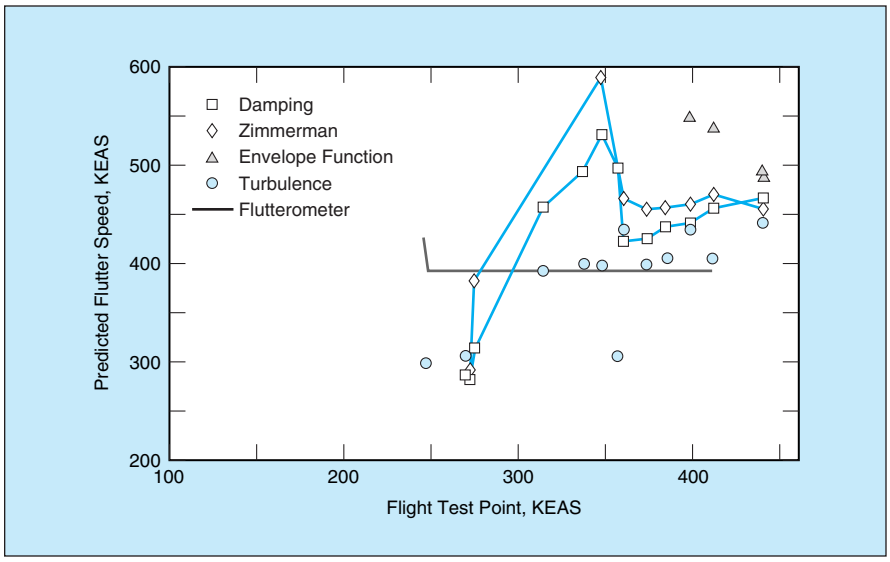

Figure 1. **Flutter Speeds** were predicted during envelope expansion by five different methods.

previous test points. The predicted speeds at the test points are plotted in Figure 1.

The predictions depicted in Figure 1 can be easily summarized. The data-based methods yield poor predictions for low-speed data but produce reasonable predictions that converge on the correct answer as the envelope is expanded to include high-speed test points. The flutterometer produces a reasonable worst-case prediction of flutter speed immediately and remains conservative throughout the envelope expansion.

An analysis of Figure 1 reveals the nature of the prediction methods. In the data-driven methods, one attempts to compute the exact speed associated with the onset of flutter. In the flutterometer (model-based) method, one attempts to obtain a conservative prediction of the worst-case flutter speed. It is expected that the data-driven methods should yield highly accurate predictions at test points close to flutter and that the particular implementation of the flutterometer should not reduce conservatism despite the analysis of data from high-speed test points.

The nature of the prediction methods indicates a method for efficient envelope expansion. A flight test should be initiated at low-speed test points and the flutterometer should be used to obtain a conservative estimate of the flutter speed. As the test proceeds, the airspeed should be increased until the system nears the speed of instability predicted by the flutterometer. At this point, the envelope should be expanded to high-speed test points by relying heavily on the data-based methods to finalize an accurate prediction of the exact speed at which flutter will be encountered.

This work was done by Rick Lind and Marty Brenner of **Dryden Flight Research Center**. *Further information is contained in a TSP (see page 1).*
DRC-01-57

Piezoelectrically Actuated Microvalve for Liquid Effluents

Power consumption and size would be reduced.

NASA's Jet Propulsion Laboratory, Pasadena, California

Modifications have been proposed to effect further improvement of the device described in "Improved Piezoelectrically Actuated Microvalve" (NPO-30158), *NASA Tech Briefs*, Vol. 26, No. 1 (January 2002), page 29. To recapitulate: What is being developed is a prototype of valves for microfluidic systems and other microelectromechanical systems (MEMS). The version of the valve reported in the cited previous article included a base (which contained a seat, an inlet, and an outlet), a diaphragm, and a linear actuator. With the exception of the actuator, the parts were micromachined from silicon. The linear actuator consisted of a stack of piezoelectric disks in a rigid housing. To make the diaphragm apply a large sealing force on the inlet and outlet, the piezoelectric stack was compressed into a slightly contracted condition during assembly of the valve. Application of a voltage across the stack caused the stack to contract into an even more compressed condition, lifting the diaphragm away from the seat, thereby creating a narrow channel between the inlet and outlet. The positions of the inlet and outlet, relative to the diaphragm and seat, were such that the inlet flow and pressure contributed to sealing and thus to a desired normally-closed mode of operation.

The basic principles of design and operation of the proposed improved valve would be the same as those of the prior valve. However, there would be important differences in design details, leading to improvements, as summarized below:

- The piezoelectric stack would be highly miniaturized (only 0.9 by 0.9 by 10 mm) and manufactured with high precision. The interior volume of the valve would be only 0.1 cm^3.
- Whereas the prior valve consumed a power of 2 W when actuated at a frequency of 100 Hz, the proposed improved version would consume only 0.1 W at 100 Hz. The combination of miniaturization and decreased power demand would be made possible by, among other things, utilization of a mode of piezoelectric actuation known in the art as d_{31}. (The term "d_{31}" signifies one of three independent moduli of piezoelectricity as well as the mode of actuation to which this modulus applies. In the d_{31} mode, the application of an electric field along one axis produces a longitudinal contraction along a perpendicular axis.)
- Unlike in the prior valve, the piezoelectric stack would be isolated from the fluid to be controlled. Hence, it would not be necessary to take special measures to protect the stack against the fluid and, even more specifically, it would not be necessary to coat the stack with a dielectric material for protection against an electrically conductive liquid.
- The design would include several features that would increase the ability of the valve to control a fluid at high pressure.

Like the prior valve, the proposed im-

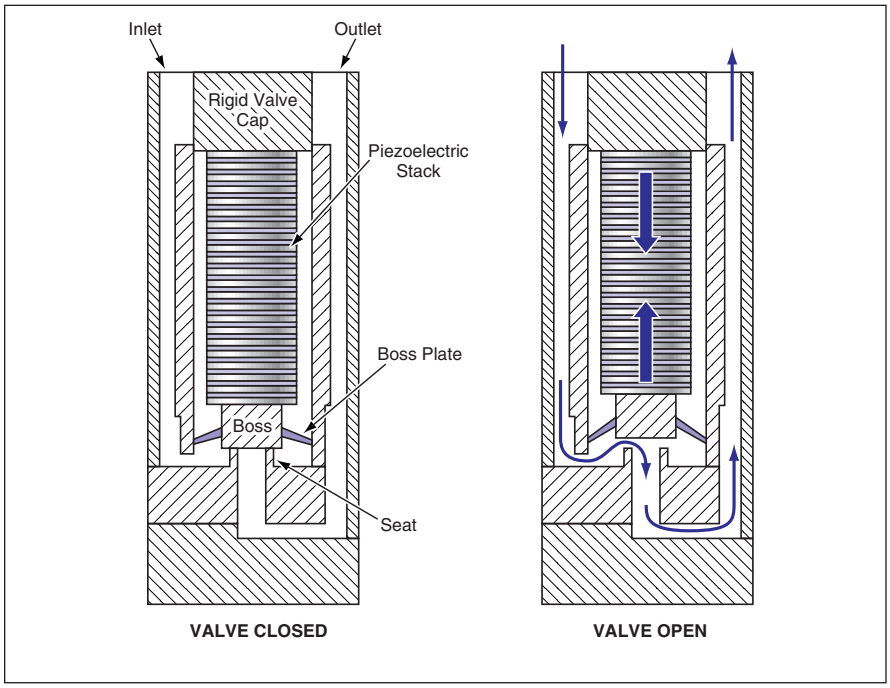

The **Valve Incorporating the Proposed Improvements** is depicted here in a simplified and partly schematic cross section, and not to scale.

proved valve (see figure) would include a base that would contain a seat, an inlet, and an outlet. The piezoelectric stack would be connected to a valve boss at one end and to a rigid valve cap at its other end. In the absence of an applied potential, the valve boss would be pressed against the valve seat, so that flow would be blocked. The application of a potential of 60 V across the stack would cause the stack to shrink, pulling the valve boss away from the seat and thereby opening a flow channel between the inlet and the outlet.

In order to increase the spring bias of the valve toward the closed position and thereby help to minimize leakage in the absence of an applied potential, the boss plate would be slightly stretched. The force generated by the piezoelectric actuator would be about 100 N — enough to overcome both the tension in the boss plate and the pressure-aided valve-closing force at an upstream-to-downstream differential pressure as large as 300 psi (≈2 MPa).

This work was done by Eui-Hyeok Yang of Caltech for **NASA's Jet Propulsion Laboratory**. *Further information is contained in a TSP (see page 1).*

In accordance with Public Law 96-517, the contractor has elected to retain title to this invention. Inquiries concerning rights for its commercial use should be addressed to

Intellectual Assets Office
JPL
Mail Stop 202-233
4800 Oak Grove Drive
Pasadena, CA 91109
(818) 354-2240
E-mail: ipgroup@jpl.nasa.gov

Refer to NPO-30562, volume and number of this NASA Tech Briefs *issue, and the page number.*

Larger-Stroke Piezoelectrically Actuated Microvalve

Liquids carrying small particles could be handled.

NASA's Jet Propulsion Laboratory, Pasadena, California

A proposed normally-closed microvalve would contain a piezoelectric bending actuator instead of a piezoelectric linear actuator like that of the microvalve described in the preceding article. Whereas the stroke of the linear actuator of the preceding article would be limited to ≈6 μm, the stroke of the proposed bending actuator would lie in the approximate range of 10 to 15 μm — large enough to enable the microvalve to handle a variety of liquids containing suspended particles having sizes up to 10 μm. Such particulate-laden liquids occur in a variety of microfluidic systems, one example being a system that sorts cells or large biomolecules for analysis.

In comparison with the linear actuator of the preceding article, the bending actuator would be smaller and less massive. The combination of increased stroke, smaller mass, and smaller volume would be obtained at the cost of decreased actuation force: The proposed actuator would

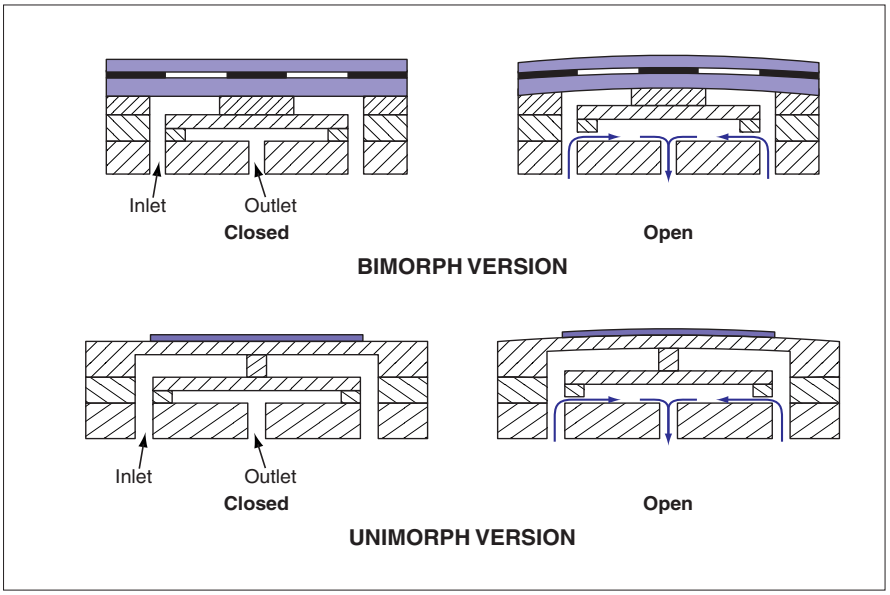

Bimorph and Unimorph Versions of a microvalve actuated by a piezoelectric bender have been proposed. The bimorph version could operate at higher pressure; the unimorph version would be more compact.

generate a force in the approximate range of 1 to 4 N, the exact amount depending on operating conditions and details of design. This level of actuation force would be too low to enable the valve to handle a fluid at the high pressure level mentioned in the preceding article.

The proposal encompasses two alternative designs — one featuring a miniature piezoelectric bimorph actuator and one featuring a thick-film unimorph piezoelectric actuator (see figure). In either version, the valve would consume a power of only 0.01 W when actuated at a frequency of 100 Hz. Also, in either version, it would be necessary to attach a soft elastomeric sealing ring to the valve seat so that any particles that settle on the seat would be pushed deep into the elastomeric material to prevent or reduce leakage.

The overall dimensions of the bimorph version would be 7 by 7 by 1 mm. The actuator in this version would generate a force of 1 N and a stroke of 10 μm at an applied potential of 150 V. The actuation force would be sufficient to enable the valve to handle a fluid pressurized up to about 50 psi (≈0.35 MPa).

The overall dimensions of the unimorph version would be 2 by 2 by 0.5 mm. In this version, an electric field across the piezoelectric film on a diaphragm would cause the film to pull on, and thereby bend, the diaphragm. At an applied potential of 20 V, the actuator in this version would generate a stroke of 10 μm and a force of 0.01 N. This force level would be too low to enable handling of fluids at pressures comparable to those of the bimorph version. This version would be useful primarily in microfluidic and nanofluidic applications that involve extremely low differential pressures and in which there are requirements for extreme miniaturization of valves. Examples of such applications include liquid chromatography and sequencing of deoxyribonucleic acid.

This work was done by Eui-Hyeok Yang of Caltech for **NASA's Jet Propulsion Laboratory**. *Further information is contained in a TSP (see page 1).*

In accordance with Public Law 96-517, the contractor has elected to retain title to this invention. Inquiries concerning rights for its commercial use should be addressed to

Intellectual Assets Office
JPL
Mail Stop 202-233
4800 Oak Grove Drive
Pasadena, CA 91109
(818) 354-2240
E-mail: ipgroup@jpl.nasa.gov

Refer to NPO-30563, volume and number of this NASA Tech Briefs *issue, and the page number.*

Innovative, High-Pressure, Cryogenic Control Valve: Short Face-to-Face, Reduced Cost

This design includes several improvements over prior designs.

Stennis Space Center, Mississippi

A control valve that can throttle high-pressure cryogenic fluid embodies several design features that distinguish it over conventional valves designed for similar applications. Field and design engineers worked together to create a valve that would simplify installation, trim changes, and maintenance, thus reducing overall cost. The seals and plug stem packing were designed to perform optimally in cryogenic temperature ranges. Unlike conventional high-pressure cryogenic valves, the trim size can be changed independent of the body.

The design feature that provides flexibility for changing the trim is a split body. The body is divided into an upper and a lower section with the seat ring sandwiched in between. In order to maintain the plug stem packing at an acceptable sealing temperature during cryogenic service, heat-exchanging fins were added to the upper body section (see figure).

The body is made of stainless steel. The seat ring is made of a nickel-based alloy having a coefficient of thermal expansion less than that of the body material. Consequently, when the interior of the valve is cooled cryogenically, the body surrounding the seat ring contracts more than the seat ring. This feature prevents external leakage at the body-seat joint. The seat ring has been machined to have small, raised-face sealing surfaces on both sides of the seal groove. These sealing surfaces concentrate the body bolt load over a small area, thereby preventing external leakage.

The design of the body bolt circle is different from that of conventional high-pressure control valves. Half of the bolts clamp the split body together from the top, and half from the bottom side. This bolt-circle design allows a short, clean flow path, which minimizes frictional flow losses. This bolt-circle design also makes it possible to shorten the face-to-face length of the valve, which is 25.5 in. (65 cm). In contrast, a conventional, high-pressure control valve face-to-face dimension may be greater than 40 in. (>1 m) long.

This work was completed by Karlin Wilkes, Ed Larsen, and Jackson McCourt of Flowserve Corporation for **Stennis Space Center**. *For further information, please contact Flowserve Corporation at (801) 489-8611 or www.flowserve.com.*

Inquiries concerning rights for the commercial use of this invention should be addressed to the Intellectual Property Manager, Stennis Space Center at (228) 688-1929. Refer to SSC-00159.

The **Split-Body Design** of this valve accommodates changes in trim. The heat-exchanger fins help keep the plug stem packing warm enough to function at cryogenic temperatures.

Safer Roadside Crash Walls Would Limit Deceleration

These walls would protect both vehicle occupants and bystanders.

Lyndon B. Johnson Space Center, Houston, Texas

The figure depicts the aspects of a proposed deceleration-limiting design for crash walls at the sides of racetracks and highways. The proposal is intended to overcome the disadvantages of both rigid barriers and kinetic-energy-absorbing barriers of prior design. Rigid barriers can keep high-speed crashing motor vehicles from leaving roadways and thereby prevent injury to nearby persons and objects, but they can also subject the occupants of the vehicles to deceleration levels high enough to cause injury or death. Kinetic-energy-absorbing barriers of prior design reduce deceleration levels somewhat, but are not designed to soften impacts optimally; moreover, some of them allow debris to bounce back onto roadways or onto roadside areas, and, in cases of glancingly incident vehicles, some of them can trap the vehicles in such a manner as to cause more injury than would occur if the vehicles were allowed to skid along the rigid barriers. The proposed crash walls would (1) allow tangentially impacting vehicles to continue sliding along the racetrack without catching them, (2) catch directly impacting vehicles to prevent them from injuring nearby persons and objects, and (3) absorb kinetic energy in a more nearly optimum way to limit decelerations to levels that human occupants could survive.

In slightly oversimplified terms, a crash wall according to the proposal would be made in segments, each segment comprising a sandwichlike structure that would contain an anchored energy-absorbing net that would capture and decelerate an impinging vehicle. The basic repeating structural unit of a net would be an energy-absorbing, load-limiting strap of a type that has been used before to dissipate kinetic energy in other settings. Such a strap is made by stitching loops in a strap made of a high-strength polymer [e.g., Kevlar (or equivalent) aromatic polyamide], such that the stitches can be ripped at a tensile load F_r somewhat less than the tensile force F_s that causes the strap to fail. When the tensile load applied to the ends of the strap reaches F_r, the loops begin to peel away and then continue to do so at a load level of $\approx F_r$ until the strap reaches the limit of its extension (at which point there are no more loops available for ripping).

The energy-absorbing straps would be connected in series to form load-limiting lanyards with strokes longer than those of individual straps. The net would contain horizontal and vertical load-limiting lanyards connected at their ends to a flexible framework of high-strength (non-load-limiting) net-support straps. At the ends of the wall segment, load-limiting lanyards would connect the lower

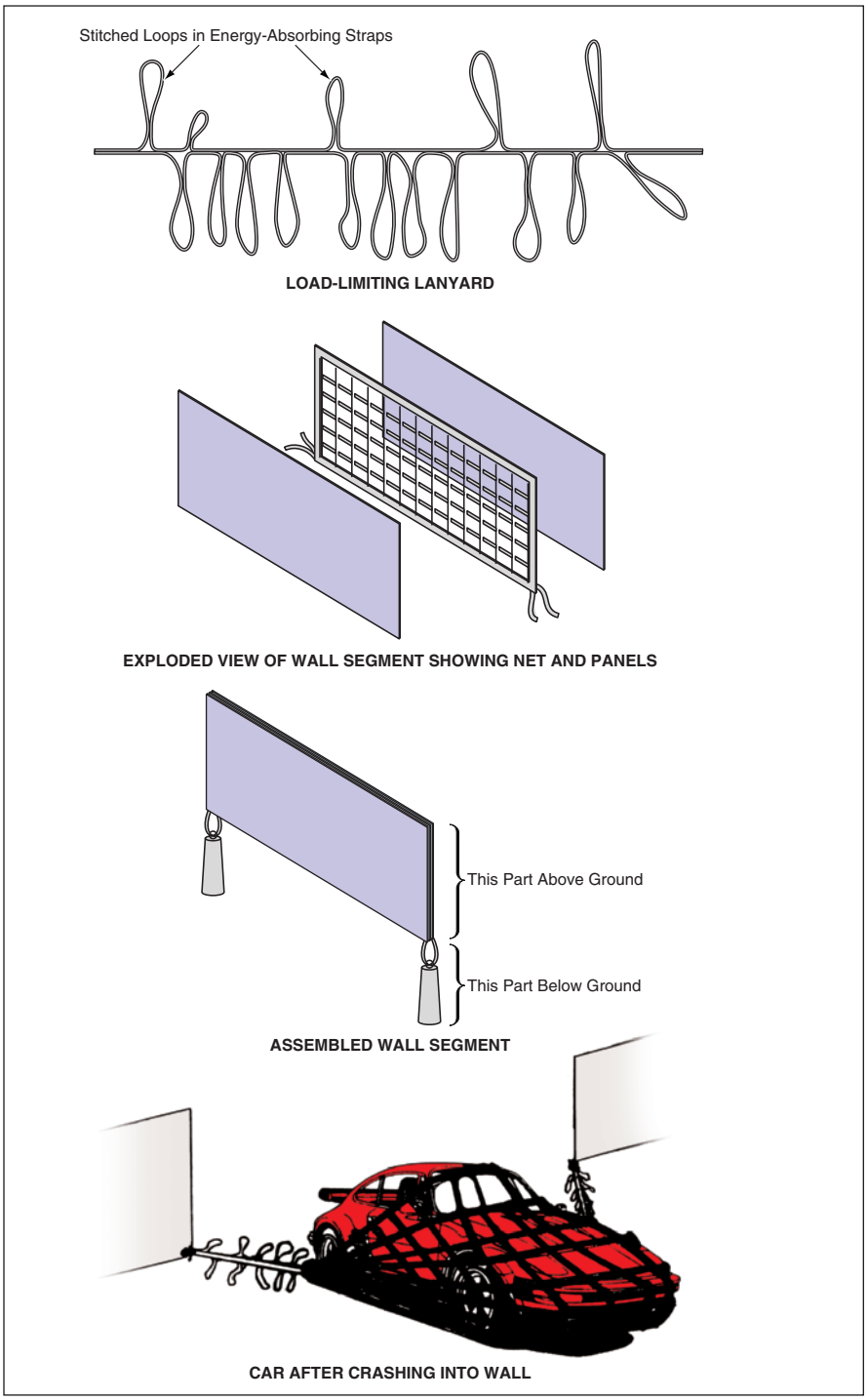

A **Load-Limiting Lanyard** would be made of series-connected energy-absorbing straps. Load-limiting lanyards would be assembled into a net. The net would be sandwiched between energy-absorbing panels and anchored to form a segment of a crash wall. The net would catch an impinging vehicle and dissipate much of its kinetic energy through ripping of the stitches in the load-limiting straps.

corners of the net to anchors buried in the ground.

The net would be sandwiched between thin energy-absorbing panels. The panel on the roadway side would be tougher than the panel on the side facing away from the road: the roadway-side panel would be capable of withstanding small impacts like those that occur many times during a race, and would be broken only by a significant impact like that of a crash. Moreover, the roadside surface of the panel could be coated with Teflon or another similar material, which would prevent tangentially impacting vehicles from breaking into the barrier. At the ends of the wall segment, a thin-walled sacrificial aluminum tube would hold the net and panels upright until a vehicle crashed into the wall. Preferably, a pair of adjacent parallel walls would be erected with the joints between their segments staggered to ensure that a vehicle crashing at any position would be stopped by at least one of the walls. The segmented construction allows for rapid post-crash cleanup and barrier repair, which is critical during televised racing events.

This work was done by William C. Schneider and James P. Locke of **Johnson Space Center**. *Further information is contained in a TSP (see page 1).*

This invention is owned by NASA, and a patent application has been filed. Inquiries concerning nonexclusive or exclusive license for its commercial development should be addressed to the Patent Counsel, Johnson Space Center, (281) 483-0837. Refer to MSC-23178.

Improved Interactive Medical-Imaging System

Complex surgery can be simulated collaboratively at multiple locations in real time.

Ames Research Center, Moffett Field, California

An improved computational-simulation system for interactive medical imaging has been invented. The system displays high-resolution, three-dimensional-appearing images of anatomical objects based on data acquired by such techniques as computed tomography (CT) and magnetic-resonance imaging (MRI). The system enables users to manipulate the data to obtain a variety of views — for example, to display cross sections in specified planes or to rotate images about specified axes. Relative to prior such systems, this system offers enhanced capabilities for synthesizing images of surgical cuts and for collaboration by users at multiple, remote computing sites.

The system (see figure) includes a database, a reconstruction unit, and a virtual collaborative clinic (VCC). The database contains data from an MRI, CT, or other scan. Within minutes of the scan, the reconstruction unit can process the data into high-resolution, stereoscopic images. The reconstruction unit includes a subunit that generates polygonal meshes to represent surfaces of anatomical objects. Whereas prior medical-imaging systems generated such meshes by means of an algorithm known in the art as the marching-cubes algorithm, this system utilizes an improved algorithm that makes it possible to reduce the computational burden of rendering surfaces at high resolution. In particular, the improved algorithm makes it possible to reduce the number of polygons drastically (by as much as 98 percent in some cases) without loss of topographical features, and without introducing spurious tears and holes, which occur in marching-cubes applications.

The reconstruction unit includes a visualization module, which processes data from the mesh generator and the database into images for display. An animation module makes it possible to generate sequences of images that show how anatomical objects change over time. A user-input module enables a user to manipulate images and control other functions by means of a mouse, trackball, touchpad, or other standard input device. Yet another module is the cyberscalpel, which, as its name suggests, enables the system to simulate cutting of an anatomical object displayed via the visualization module.

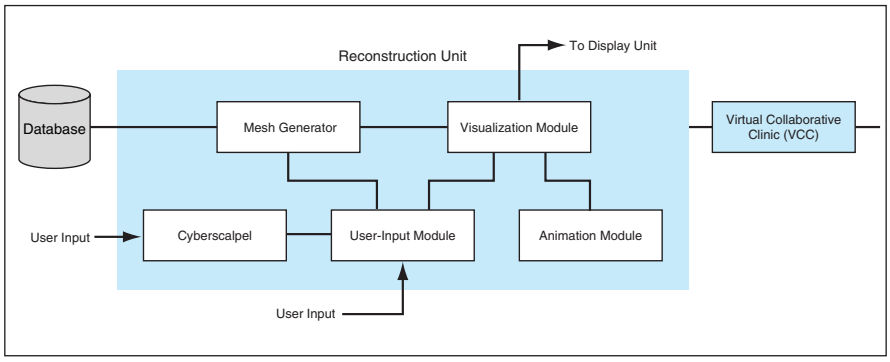

This **Interactive Medical-Imaging System** can be implemented in hardware and/or software.

The VCC is an extension of the reconstruction unit. The VCC can include counterpart components that reside on separate computers at multiple remote locations, enabling users at those locations to interact with the same simulated anatomical objects in real time. The data structure of the system provides for sharing, among the geographically dispersed computers, of a number of variables and of computational models that represent anatomical objects at various levels of image resolution. Data are multicast among the computers on the basis of the data structure, such that by means of the multicast data and a provision for dynamic selection among the computational models, the same images can be displayed on all the computers. For example, all users can observe a simulated surgical cut performed by one of the users. Thus, surgeons at multiple locations can collaborate in planning complicated surgery in advance, using realistic displays.

This work was done by Muriel D. Ross, Ian A. Twombly, and Steven Senger of **Ames Research Center**.

Inquiries concerning rights for the commercial use of this invention should be addressed to the Patent Counsel, Ames Research Center, (650) 604-5104. Refer to ARC-14441.

Scanning Microscopes Using X Rays and Microchannels

In principle, resolutions of the order of nanometers could be attained.

NASA's Jet Propulsion Laboratory, Pasadena, California

Scanning microscopes that would be based on microchannel filters and advanced electronic image sensors and that utilize x-ray illumination have been proposed. Because the finest resolution attainable in a microscope is determined by the wavelength of the illumination, the x-ray illumination in the proposed microscopes would make it possible, in principle, to achieve resolutions of the order of nanometers — about a thousand times as fine as the resolution of a visible-light microscope. Heretofore, it has been necessary to use scanning electron microscopes to obtain such fine resolution. In comparison with scanning electron microscopes, the proposed microscopes would likely be smaller, less massive, and less expensive. Moreover, unlike in scanning electron microscopes, it would not be necessary to place specimens under vacuum.

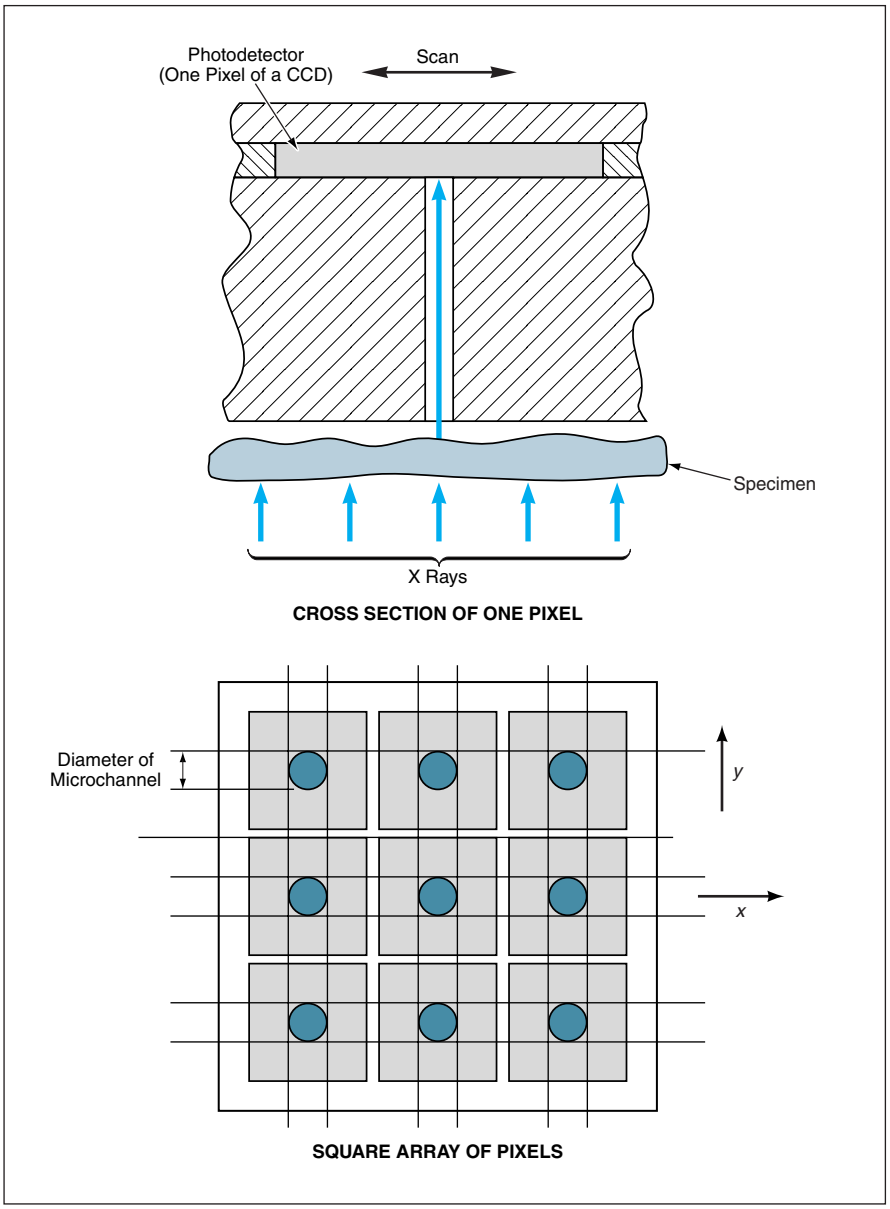

X-Rays From the Specimen would travel through the microchannels to the photodetectors. The microchannels would define resolution elements. In both the x and y directions, the microchannel plate and photodetectors would be scanned over one pixel pitch, in increments of the microchannel diameter, to acquire high-resolution specimen-image data.

The proposed microscopes are closely related to the ones described in several prior *NASA Tech Briefs* articles; namely, "Miniature Microscope Without Lenses" (NPO-20218), *NASA Tech Briefs*, Vol. 22, No. 8 (August 1998), page 43; and "Reflective Variants of Miniature Microscope Without Lenses" (NPO-20610), *NASA Tech Briefs*, Vol. 26, No. 9 (September 2002) page 6a. In all of these microscopes, the basic principle of design and operation is the same:

The focusing optics of a conventional visible-light microscope are replaced by a combination of a microchannel filter and a charge-coupled-device (CCD) image detector. A microchannel plate containing parallel, microscopic-cross-section holes much longer than they are wide is placed between a specimen and an image sensor, which is typically the CCD. The microchannel plate must be made of a material that absorbs the illuminating radiation reflected or scattered from the specimen. The microchannels must be positioned and dimensioned so that each one is registered with a pixel on the image sensor. Because most of the radiation incident on the microchannel walls becomes absorbed, the radiation that reaches the image sensor consists predominantly of radiation that was launched along the longitudinal direction of the microchannels. Therefore, most of the radiation arriving at each pixel on the sensor must have traveled along a straight line from a corresponding location on the specimen. Thus, there is a one-to-one mapping from a point on a specimen to a pixel in the image sensor, so that the output of the image sensor contains image information equivalent to that from a microscope.

The upper part of the figure depicts a one-pixel portion of a proposed scanning microchannel-type microscope that would utilize x-ray illumination. The lower part of the figure shows a simple square pixel pattern. The CCD could be coated with a phosphor to increase its response to x-ray photons. Provided that the

x-ray wavelength was small enough, the diameter of the microchannel would define the resolution element. The microchannels would be much narrower than the CCD pixels. Preferably, the pixel pitch would be an integer multiple of the diameter of a microchannel. Hence, one would acquire a set of high-resolution image data by recording the CCD output while scanning (more precisely, stepping) the specimen under the microchannel plate in increments of the microchannel diameter along both perpendicular axes (x and y) of the pixel pattern.

This work was done by Yu Wang of Caltech for **NASA's Jet Propulsion Laboratory**. *Further information is contained in a TSP (see page 1).* *NPO-20873*

Slotting Fins of Heat Exchangers To Provide Thermal Breaks

Lyndon B. Johnson Space Center, Houston, Texas

Heat exchangers that include slotted fins (in contradistinction to continuous fins) have been invented. The slotting of the fins provides thermal breaks that reduce thermal conduction along flow paths (longitudinal thermal conduction), which reduces heat-transfer efficiency. By increasing the ratio between transverse thermal conduction (the desired heat-transfer conduction) and longitudinal thermal conduction, slotting of the fins can be exploited to (1) increase heat-transfer efficiency (thereby reducing operating cost) for a given heat-exchanger length or to (2) reduce the length (thereby reducing the weight and/or cost) of the heat exchanger needed to obtain a given heat-transfer efficiency. By reducing the length of a heat exchanger, one can reduce the pressure drop associated with the flow through it. In a case in which slotting enables the use of fins with thermal conductivity greater than could otherwise be tolerated on the basis of longitudinal thermal conduction, one can exploit the conductivity to make the fins longer (in the transverse direction) than they otherwise could be, thereby making it possible to make a heat exchanger that contains fewer channels and therefore, that weighs less, contains fewer potential leak paths, and can be constructed from fewer parts and, hence, reduced cost.

This work was done by Timothy D. Scull of United Technologies for **Johnson Space Center**. *For more information, contact the Johnson Commercial Technology Office at (281) 483-3809.*
MSC-22784

Methane Clathrate Hydrate Prospecting

Methane hydrate deposits would be detected indirectly through thermal, magnetic, and electric measurements.

NASA's Jet Propulsion Laboratory, Pasadena, California

A method of prospecting for methane has been devised. The impetus for this method lies in the abundance of CH_4 and the growing shortages of other fuels. The method is intended especially to enable identification of subpermafrost locations where significant amounts of methane are trapped in the form of methane gas hydrate ($CH_4 \cdot 6H_2O$). It has been estimated by the U.S. Geological Survey that the total CH_4 resource in $CH_4 \cdot 6H_2O$ exceeds the energy content of all other fossil fuels (oil, coal, and natural gas from non-hydrate sources). Also, $CH_4 \cdot 6H_2O$ is among the cleanest-burning fuels, and CH_4 is the most efficient fuel because the carbon in CH_4 is in its most reduced state. The method involves looking for a proxy for methane gas hydrate, by means of the combination of a thermal-analysis submethod and a field submethod that does not involve drilling. The absence of drilling makes this method easier and less expensive, in comparison with prior methods of prospecting for oil and natural gas.

The proposed method would include thermoprospecting in combination with one more of the other non-drilling measurement techniques, which could include magneto-telluric sounding and/or a subsurface-electrical-resistivity technique. The method would exploit the fact that the electrical conductivity in the underlying thawed region is greater than that in the overlying permafrost.

This work was done by N. Duxbury of Caltech and V. Romanovsky of the University of Alaska at Fairbanks for **NASA's Jet Propulsion Laboratory**. *For further information, access the Technical Support Package (TSP)* ***free on-line at www.techbriefs.com/tsp*** *under the Physical Sciences category.*
NPO-30257

Automated Monitoring With a BSP Fault-Detection Test

This test is sensitive to subtle statistical changes in monitored signals.

Marshall Space Flight Center, Alabama

The figure schematically illustrates a method and procedure for automated monitoring of an asset, as well as a hardware-and-software system that implements the method and procedure. As used here, "asset" could signify an industrial process, power plant, medical instrument, aircraft, or any of a variety of other systems that generate electronic signals (e.g., sensor outputs). In automated monitoring, the signals are digitized and then processed in order to detect faults and otherwise monitor operational status and integrity of the monitored asset. The major distinguishing feature of the present method is that the fault-detection function is implemented by use of a Bayesian sequential probability (BSP) technique. This technique is superior to other techniques for automated monitoring because it affords sensitivity, not only to disturbances in the mean values, but also to very subtle changes in the statistical characteristics (variance, skewness, and bias) of the monitored signals.

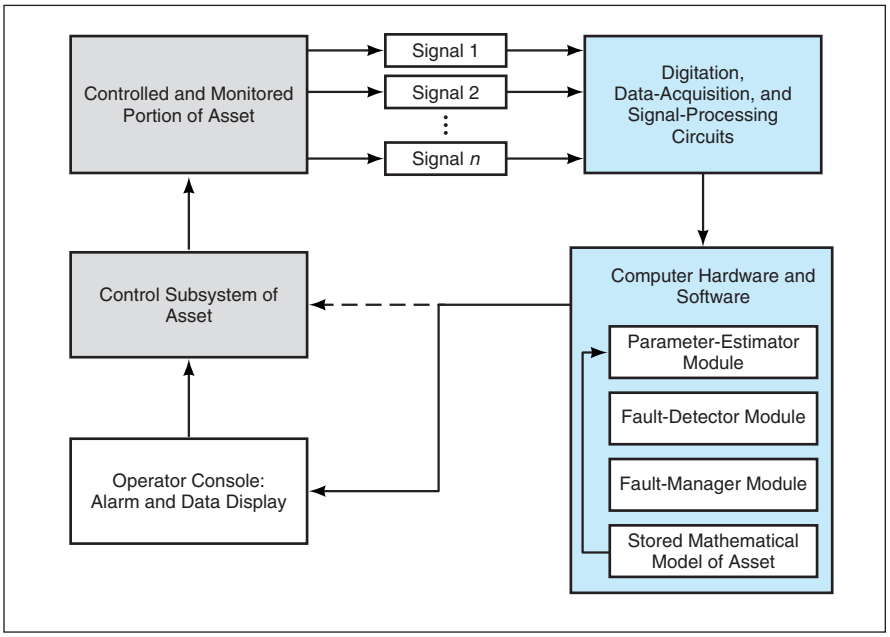

Monitoring of an Asset is Automated by a method that incorporates the BSP technique. This method affords sensitivity to subtle changes in statistical characteristics of signals and yields fewer fault-decision errors than does a prior method that incorporates the SPRT technique.

In one version of the method, what are monitored are one or more signals from the asset, along with estimates of the signals generated by a parameter-estimator module that uses a stored mathematical model of the asset. In another version of the method, what are monitored are two nominally redundant signals from the asset. In both versions, the differences between corresponding monitored signals are quantified in a residual-error value that is then used for fault detection. A fault-detector module implements the present BSP technique to determine whether the residual-error value is indicative of a signal or asset fault. Next, a fault-manager module decides, on the basis of a series of results generated by the fault-detector module, whether a fault is present. This fault decision is communicated to an operator or to the control subsystem of the asset for corrective action.

In this method, the BSP technique is embodied in a statistical fault-detection algorithm for detecting changes in a residual-error signal. The BSP technique involves the BSP test, which is a statistical hypothesis test that differs, from the classical fixed-sample hypothesis test, in the way in which statistical observations are employed. In the fixed-sample hypothesis test, a given number of observations are used to select one hypothesis from two or more alternatives. In the BSP test, one examines observations dynamically, one at a time, and selects a hypothesis when adequate evidence is obtained from the series of observations.

The predecessor of the present fault-detection method incorporating the BSP technique is a fault-detection method that incorporates another dynamic statistical fault-detection test known as the sequential probability ratio test (SPRT). A significant shortcoming of SPRT technique is found in the assumptions underlying its mathematical formulation. Specifically, the SPRT technique incorporates the assumption that the residual-error signals are characterized by a Gaussian probability-density function. For residual-error signals that are non-Gaussian, the fault-detector module of the SPRT technique yields unacceptably large false- and missed-alarm rates.

In contrast, in the present method, it is not assumed that the residual-error signals are characterized by a Gaussian probability-density function. Instead, the BSP technique involves the use of any of a number of other techniques for numerically fitting a probability-density function to a residual-error signal distribution that is characteristic of normal operation of the asset. The probability-density function thus derived is then used in the dynamic statistical hypothesis test. As a result, rates of false and missed alarms are smaller; in other words, fault decisions tend to be more accurate than they are in the SPRT technique.

This work was done by Randall L. Bickford of Expert Microsystems, Inc., and James P. Herzog of Argonne National Laboratory for **Marshall Space Flight Center**. *This technology is immediately available using the SureSense™ Signal Validation System software produced by Expert Microsystems, Inc. For more information, contact the company at (916) 989-2018 or at expert@expmicrosys.com.*

MFS-31590

Automated Monitoring With a BCP Fault-Decision Test

Fault-detection events are evaluated to reduce the incidence of false alarms.

Marshall Space Flight Center, Alabama

The Bayesian conditional probability (BCP) technique is a statistical fault-decision technique that is suitable as the mathematical basis of the fault-manager module in the automated-monitoring system and method described in the immediately preceding article. Within the automated-monitoring system, the fault-manager module operates in conjunction with the fault-detector module, which can be based on any one of several fault-detection techniques; examples include a threshold-limit-comparison technique or the BSP or SPRT technique mentioned in the preceding article. The present BCP technique is used to evaluate a series of one or more fault-detection events for the purpose of filtering out occasional false alarms produced by many types of statistical fault-detection procedures. The BCP technique increases the probability that an automated monitoring system produces a correct decision regarding the presence or absence of a fault.

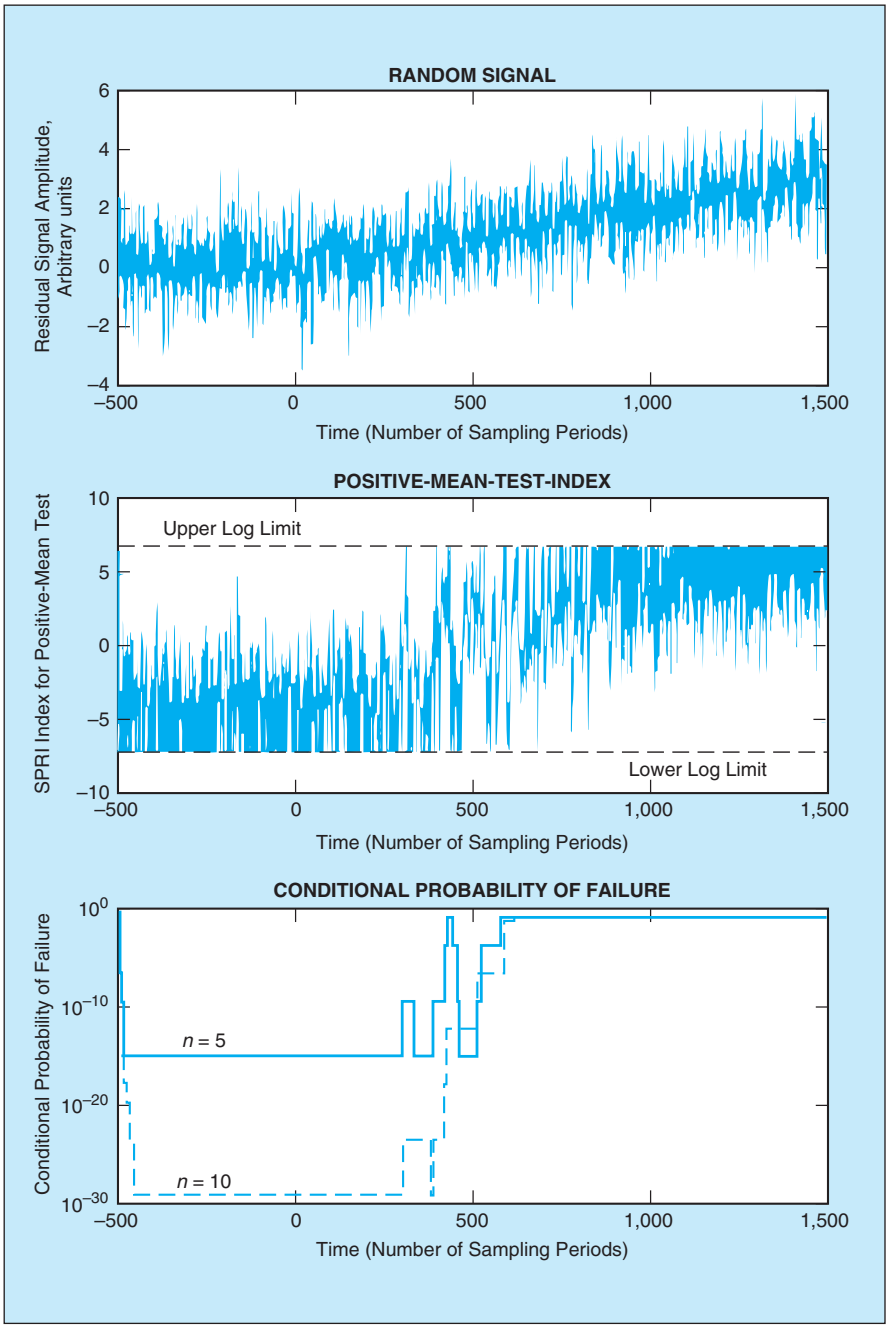

These **Plots Were Generated** in an application of the BCP technique, in conjunction with the SPRT technique, to data from a simulated sensor failure that manifested itself in a slow drift of the sensor output. As soon as the number of "fault" decisions reached by the SPRT exceeded the number of "normal" decisions, the conditional probability exceeded a confidence level, causing the BCP test to conclude that a failure had occurred.

Because occasional false alarms are an inevitable consequence of the SPRT, BSP, or any other statistically based fault-detection test, there is a need for a logical procedure to distinguish between true and false alarms. Heretofore, it has been common practice to make a fault decision on an *ad hoc* basis — for example, by following a multiple-observation voting strategy in which a signal is declared to be indicative of a fault if m of the last n observations produced a fault-detection alarm. The BCP technique was developed to obtain results more reliable than those afforded by a voting strategy.

The BCP technique involves a test in which one applies Bayesian inference techniques to a series of one or more single-observation alarms produced by a fault-detection test. One considers the last n decisions generated by a fault-detection test in order to evaluate the conditional probability that a failure is indicated (see figure). Each new decision reached by a fault-detection test is treated as a new piece of evidence about the state of the monitored asset, and the conditional probability of failure for the system is updated on the basis of this new evidence. The conditional probability of failure is compared with a predefined limit. For a probability below the limit, the asset is declared to be healthy. For a probability above the limit, the asset is declared to be faulty.

This work was done by Randall L. Bickford of Expert Microsystems, Inc., and James P. Herzog of Argonne National Laboratory for **Marshall Space Flight Center.** *This technology is immediately available using the SureSense™ Signal Validation System software produced by Expert Microsystems, Inc. For more information, contact the company at (916) 989-2018 or at expert@expmicrosys.com.*
MFS-31589

Vector-Ordering Filter Procedure for Data Reduction

The essential characteristics of original large sets of data are preserved.

Marshall Space Flight Center, Alabama

The vector-ordering filter (VOF) technique involves a procedure for sampling a large population of data vectors to select a subset of data vectors that fully characterize the state space of the large population. The VOF technique enables a large reduction of the volume of data that must be handled in the automated-monitoring system and method discussed in the two immediately preceding articles. In so doing, the VOF technique enables the development of data-driven mathematical models of a monitored asset from sets of data that would otherwise exceed the memory capacities of conventional engineering computers.

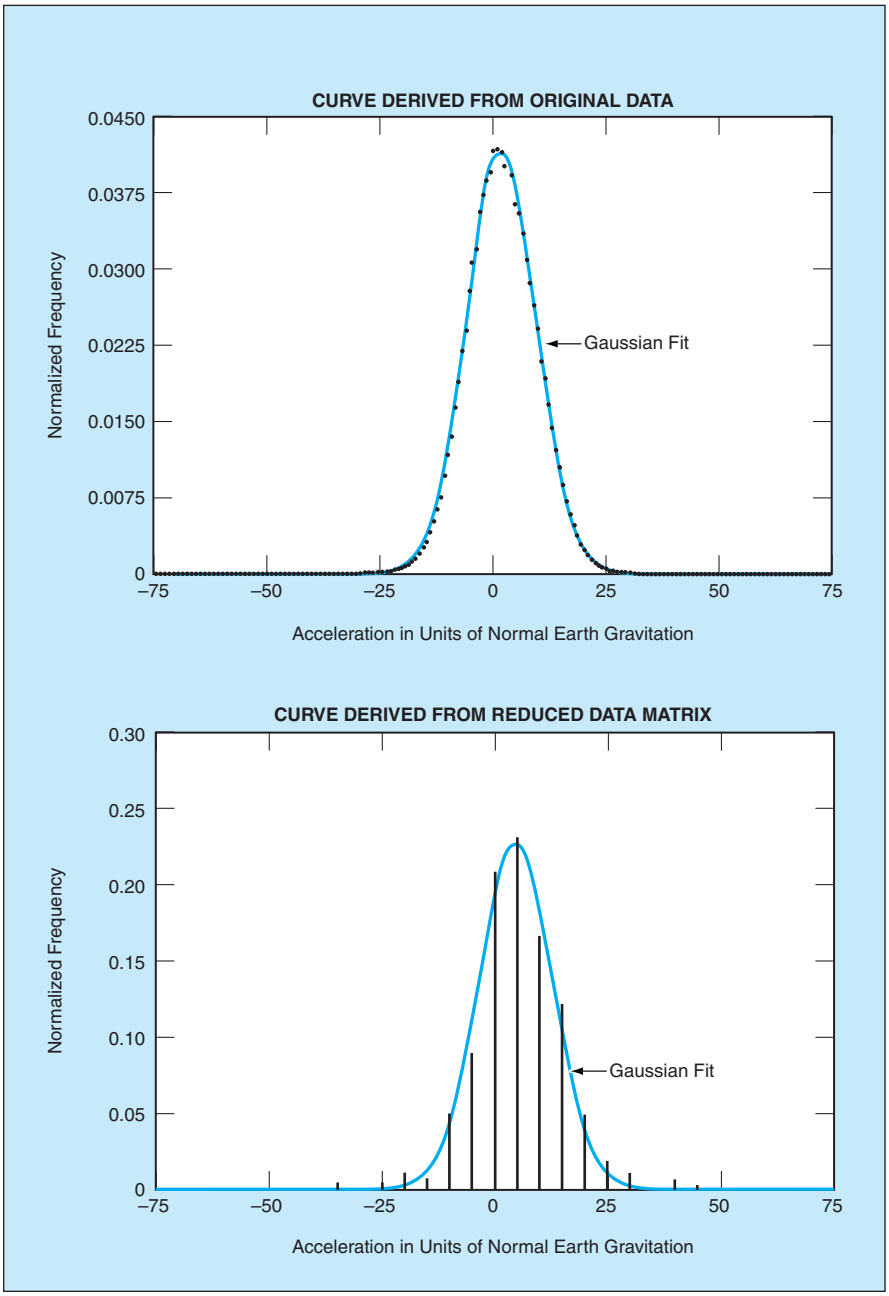

These **Plots Characterize Data** from an original data matrix and a reduced data matrix derived from it in two VOF passes. The original set of data represented 62,914,252 observations, each observation comprising readings of 6 accelerometers on the space shuttle main engine. The first VOF pass, made over 394 subsets of the original data, yielded a reduced data matrix of 160,358 vectors. The second pass extracted a final reduced data matrix containing 250 vectors.

Data-driven mathematical models have been shown to offer high fidelity for purposes of control and monitoring of assets. In practice, a collection of asset-operating observations is acquired with the intention that the collection contain observations characteristic of the full dynamic range of operation of the asset. Often, such a collection contains an extremely large number of observations, many of which are redundant. The VOF technique fills the need for a means to extract, from the original collection of observational data, a reduced data matrix that excludes redundant data while maintaining the full statistical character and dynamic range of the original data. The reduced data matrix can then be used as the input data for development of a mathematical model of the monitored asset, or as training data for a neural-network substitute for an explicit mathematical model of the asset. Alternatively, the reduced data matrix can, itself, be used directly as a mathematical model of the monitored asset, as is commonly done in multivariate state-estimation techniques.

The original data are collected from the asset over a range of operating states and are put in matrix form. Each column vector in the original data matrix represents the signal values acquired at a particular operational state of the asset. Thus, the number of columns of the original data matrix equals the number of observed states and the number of rows in this matrix equals the number of signals acquired at each observation. In the VOF technique, one extracts the reduced data matrix from the original data matrix through the selection of a representative subset of the column (state) vectors.

In its simplest form, the VOF procedure is a two-stage procedure, in the first stage of which one selects those data vectors that characterize the extrema present in the original data. At the beginning of the first stage, one finds the extrema of each signal as represented by the minimum and maximum values in the corresponding row of the original data matrix. The column vectors that contain these values are selected as candidates for inclusion in the reduced data matrix. Before a candidate column vector is added to the reduced data matrix,

it is compared with those column vectors already in the reduced data matrix to ensure that only one copy of that vector ends up in the reduced data matrix. In the second stage, one orders the column vectors of the original data matrix by their Euclidean norms and then selects a subset of the vectors according to a spacing criterion. All column vectors selected in this way are compared to those vectors selected during the first stage. Only those column vectors that were not already included in the reduced data matrix during the first stage are added to the reduced data matrix.

Practical sets of data tend to be so large that excessive computer memory would be necessary for a single pass of the two-stage VOF procedure over all the data. In such a case, the VOF procedure can be applied recursively to successive subsets of the original data that are small enough to fit in the available memory. The figure presents plots from an example of a two-pass application of the VOF technique to some space-shuttle engine vibration data.

This work was done by Randall L. Bickford of Expert Microsystems, Inc., and James P. Herzog of Argonne National Laboratory for **Marshall Space Flight Center**. *This technology is immediately available using the SureSense™ Signal Validation System software produced by Expert Microsystems, Inc. For more information, contact the company at (916) 989-2018 or at expert@expmicrosys.com.*
MFS-31588

Remote Sensing and Information Technology for Large Farms

Timely data on spatial and temporal variations in fields help farmers manage crops.

Stennis Space Center, Mississippi

A method of applying remote sensing (RS) and information-management technology to help large farms produce at maximum efficiency is undergoing development. The novelty of the method does not lie in the concept of "precision agriculture," which involves variation of seeding, of application of chemicals, and of irrigation according to the spatially and temporally local variations in the growth stages and health of crops and in the chemical and physical conditions of soils. The novelty also does not lie in the use of RS data registered with other data in a geographic information system (GIS) to guide the use of precise agricultural techniques. Instead, the novelty lies in a systematic approach to overcoming obstacles that, heretofore, have impeded the timely distribution of reliable, relevant, and sufficient GIS data to support day-to-day, acre-to-acre decisions concerning the application of precise agricultural techniques to increase production and decrease cost.

The development and promotion of the method are inspired in part by a vision of equipping farm machinery to accept GIS (including RS) data and using the data for automated or semi-automated implementation of precise agricultural techniques. Primary examples of relevant GIS data include information on plant stress, soil moisture, and effects of applied chemicals, all derived by automated computational analysis of measurements taken by one or more airborne spectroradiometers.

Proper management and timeliness of the large amount of GIS information are of paramount concern in agriculture. Information on stresses and changes in crops is especially perishable and important to farmers. The need for timeliness and management of information is satisfied by use of computing hardware and software capable of (1) rapid geo-rectification and other processing of RS data, (2) packaging the output data in the form of GIS plots, and (3) making the data available to farmers and other subscribers by Internet password access. It is a goal of this development program to make RS data available no later than the data after an aerial survey. In addition, data from prior surveys are kept in the data base. Farmers can, for example, use current and prior data to analyze changes.

This work was done by John E. Williams of Global Positioning Solutions, Inc., and Jimmie A. Ramsay of DataStar, Inc. for **Stennis Space Center**.

In accordance with Public Law 96-517, the contractor has elected to retain title to this invention. Inquiries concerning rights for its commercial use should be addressed to:

Global Positioning Solutions, Inc.
P.O. Box 89
Inverness, MS 38753

Refer to SSC-00150, volume and number of this NASA Tech Briefs *issue, and the page number.*

Books & Reports

Developments at the Advanced Design Technologies Testbed

A report presents background and historical information, as of August 1998, on the Advanced Design Technologies Testbed (ADTT) at Ames Research Center. The ADTT is characterized as an activity initiated to facilitate improvements in aerospace design processes; provide a proving ground for product-development methods and computational software and hardware; develop "bridging" methods, software, and hardware that can facilitate integrated solutions to design problems; and disseminate lessons learned to the aerospace and information-technology communities.

This work was done by William R. Van Dalsem, Mary E. Livingston, John E. Melton, Francisco J. Torres, and Paul M. Stremel of **Ames Research Center**. *Further information is contained in a TSP (see page 1).*

Inquiries concerning rights for the commercial use of this invention should be addressed to the Patent Counsel, Ames Research Center, (650) 604-5104. Refer to ARC-14303-1.

Spore-Forming Bacteria That Resist Sterilization

A report presents a phenotypic and genotypic characterization of a bacterial species that has been found to be of the genus *Bacillus* and has been tentatively named *B. odysseensis* because it was isolated from surfaces of the Mars Odyssey spacecraft as part of continuing research on techniques for sterilizing spacecraft to prevent contamination of remote planets by terrestrial species. *B. odysseensis* is a Gram-positive, facultatively anaerobic, rod-shaped bacterium that forms round spores. The exosporium has been conjectured to play a role in the elevated resistance to sterilization. Research on the exosporium is proposed as a path toward improved means of sterilization, medical treatment, and prevention of biofouling.

This work was done by Myron La Duc and Kasthuri Venkateswaran of Caltech for **NASA's Jet Propulsion Laboratory**. *Further information is contained in a TSP (see page 1).*

In accordance with Public Law 96-517, the contractor has elected to retain title to this invention. Inquiries concerning rights for its commercial use should be addressed to:

Innovative Technology Assets Management
JPL
Mail Stop 202-233
4800 Oak Grove Drive
Pasadena, CA 91109-8099
(818) 354-2240
E-mail: iaoffice@jpl.nasa.gov

Refer to NPO-40041, volume and number of this NASA Tech Briefs *issue, and the page number.*

Acoustical Applications of the HHT Method

A document discusses applications of a method based on the Huang-Hilbert transform (HHT). The method was described, without the HHT name, in "Analyzing Time Series Using EMD and Hilbert Spectra" (GSC-13817), *NASA Tech Briefs*, Vol. 24, No. 10 (October 2000), page 63. To recapitulate: The method is especially suitable for analyzing time-series data that represent nonstationary and nonlinear physical phenomena. The method involves the empirical mode decomposition (EMD), in which a complicated signal is decomposed into a finite number of functions, called "intrinsic mode functions" (IMFs), that admit well-behaved Hilbert transforms. The HHT consists of the combination of EMD and Hilbert spectral analysis.

This work was done by Norden E. Huang of **Goddard Space Flight Center**. *Further information is contained in a TSP (see page 1).*

This invention is owned by NASA, and a patent application has been filed. Inquiries concerning nonexclusive or exclusive license for its commercial development should be addressed to the Patent Counsel, Goddard Space Flight Center; (301) 286-7351. Refer to GSC-13817-4.


NASA
National Aeronautics and
Space Administration